



Contents lists available at ScienceDirect

Quaternary Science Reviews

journal homepage: www.elsevier.com/locate/quascirev



Paleoclimatic and paleoceanographic records through Marine Isotope Stage 19 at the Chiba composite section, central Japan: A key reference for the Early–Middle Pleistocene Subseries boundary

Yusuke Suganuma^{a, b, *}, Yuki Haneda^c, Koji Kameo^d, Yoshimi Kubota^e, Hiroki Hayashi^f, Takuya Itaki^g, Masaaki Okuda^h, Martin, J. Headⁱ, Manami Sugaya^j, Hiroomi Nakazato^k, Atsuo Igarashi^l, Kizuku Shikoku^f, Misao Hongo^m, Masami Watanabeⁿ, Yasufumi Satoguchi^o, Yoshihiro Takeshita^p, Naohisa Nishida^q, Kentaro Izumi^r, Kenji Kawamura^{a, b}, Moto Kawamata^b, Jun'ichi Okuno^{a, b}, Takeshi Yoshida^s, Itaru Ogitsu^s, Hisashi Yabusaki^s, Makoto Okada^c

^a National Institute of Polar Research, 10-3 Midori-cho, Tachikawa, Tokyo, 190-8518, Japan

^b Department of Polar Science, School of Multidisciplinary Sciences, The Graduate University for Advanced Studies (SOKENDAI), Midori-cho 10-3, Tachikawa, Tokyo, 190-8518, Japan

^c Department of Earth Sciences, Ibaraki University, 2-2-1 Bunkyo, Mito, Ibaraki, 310-8512, Japan

^d Department of Earth Sciences, Chiba University, 1-33 Yayoi, Inage, Chiba, Chiba, 263-8522, Japan

^e Department of Geology and Paleontology, National Museum of Nature and Science, 4-1-1 Amakubo, Tsukuba, Ibaraki, 305-0005, Japan

^f Interdisciplinary Graduate School of Science and Engineering, Shimane University, Nishikawatsucho 1060, Matsue, Shimane, 690-8504, Japan

^g Geological Survey of Japan, AIST, Tsukuba Central 7, 1-1-1 Hagashi, Tsukuba, Ibaraki, 305-8567, Japan

^h Natural History Museum and Institute, Chiba, 955-2 Aoba-cho, Chuo, Chiba, 260-8682, Japan

ⁱ Department of Earth Sciences, 1812 Sir Isaac Brock Way, Brock University, Ontario, L2S 3A1, Canada

^j Giken Consul., Ltd., 1-15-3 Shimokoide, Maebashi, Gunma, 371-0031, Japan

^k Institute for Rural Engineering, NARO, 2-1-6 Kannondai, Tsukuba, Ibaraki, 305-8609, Japan

^l Fukken Co., Ltd. Tokyo Branch Office, 3-8-15 Iwamoto-cho, Chiyoda, Tokyo, 101-0032, Japan

^m Alps Technical Research Laboratory Co., Ltd., 2287-27 Toyoshina-takibe, Azumino, Nagano, 399-8204, Japan

ⁿ Archaeological Research Consultant, Inc., 131 Shimohigashikawatsu, Matsue, 690-0822, Japan

^o Lake Biwa Museum, 1091 Oroshimo-cho, Kusatsu, 525-0001, Japan

^p Institute of Education, Shinshu University, 6-ro Nishinagano, Nagano 380-8544, Japan

^q Department of Environmental Sciences, Tokyo Gakugei University, 4-1-1 Nukuikita, Koganei, Tokyo, 184-8501, Japan

^r Faculty and Graduate School of Education, Chiba University, 1-33 Yayoi-cho, Inage, Chiba, Chiba, 263-8522, Japan

^s Research Institute of Environmental Geology, Chiba, 3-5-1 Inagekaigan, Mihama, Chiba, 261-0005, Japan

ARTICLE INFO

Article history:

Received 4 April 2017

Received in revised form

6 April 2018

Accepted 23 April 2018

Available online 29 May 2018

Keywords:

Marine Isotope Stage (MIS) 19

Oxygen isotope ($\delta^{18}\text{O}$) stratigraphy

Pollen

ABSTRACT

Marine Isotope Stage (MIS) 19 is an important analogue for the present interglacial because of its similar orbital configuration, especially the phasing of the obliquity maximum to precession minimum. However, sedimentary records suitable for capturing both terrestrial and marine environmental changes are limited, and thus the climatic forcing mechanisms for MIS 19 are still largely unknown. The Chiba composite section, east-central Japanese archipelago, is a continuous and expanded marine sedimentary succession well suited to capture terrestrial and marine environmental changes through MIS 19. In this study, a detailed oxygen isotope chronology is established from late MIS 20 to early MIS 18, supported by a U-Pb zircon age and the presence of the Matuyama–Brunhes boundary. New pollen, marine microfossil, and planktonic foraminiferal $\delta^{18}\text{O}$ and Mg/Ca paleotemperature records reveal the complex interplay of climatic influences. Our pollen data suggest that the duration of full interglacial conditions

* Corresponding author. National Institute of Polar Research, 10Midori-cho, Tachikawa, Tokyo, 190, Japan.

E-mail addresses: suganuma.yusuke@nipr.ac.jp (Y. Suganuma), yuuki.haneda.paleo@gmail.com (Y. Haneda), kameo@faculty.chiba-u.jp (K. Kameo), yoshimi@kahaku.go.jp (Y. Kubota), hayashi@riko.shimane-u.ac.jp (H. Hayashi), t-itaki@aist.go.jp (T. Itaki), okuda@chiba-muse.or.jp (M. Okuda), mjhead@brocku.ca (M.J. Head), mana.artemisia@gmail.com (M. Sugaya), h_nakazato@affrc.go.jp (H. Nakazato), igarashi@fukken.co.jp (A. Igarashi), mitutomimika@yahoo.co.jp (K. Shikoku), misao-alps@mint.odn.ne.jp (M. Hongo), info@cons-ar.co.jp (M. Watanabe), satoguchi-yasufumi@biwahaku.jp (Y. Satoguchi), takey@shinshu-u.ac.jp (Y. Takeshita), nishidan@u-gakugei.ac.jp (N. Nishida), izumi@chiba-u.jp (K. Izumi), kawamura@nipr.ac.jp (K. Kawamura), kawamata.moto@nipr.ac.jp (M. Kawamata), okuno@nipr.ac.jp (J. Okuno), t.yshd61@pref.chiba.lg.jp (T. Yoshida), i.logts@pref.chiba.lg.jp (I. Ogitsu), h.ybsk4@pref.chiba.lg.jp (H. Yabusaki), makoto.okada.sci@vc.ibaraki.ac.jp (M. Okada).

Foraminifera
 Calcareous nannofossils
 Radiolarians
 Mg/Ca
 Matuyama–Brunhes boundary
 Chiba composite section (CbCS)
 Lower–Middle Pleistocene boundary

during MIS 19 extends from 785.0 to 775.1 ka (9.9 kyr), which offers an important natural baseline in predicting the duration of the present interglacial. A Younger Dryas-type cooling event is present during Termination IX, suggesting that such events are linked to this orbital configuration. Millennial- to multi-millennial-scale variations in our $\delta^{18}\text{O}$ and Mg/Ca records imply that the Subarctic Front fluctuated in the northwestern Pacific Ocean during late MIS 19, probably in response to East Asian winter monsoon variability. The climatic setting at this time appears to be related to less severe summer insolation minima at 65N and/or high winter insolation at 50N. Our records do not support a recently hypothesized direct coupling between variations in the geomagnetic field intensity and global/regional climate change. Our highly resolved paleoclimatic and paleoceanographic records, coupled with a well-defined Matuyama–Brunhes boundary (772.9 ka; duration 1.9 kyr), establish the Chiba composite section as an exceptional climatic and chronological reference section for the Early–Middle Pleistocene boundary.

© 2018 The Authors. Published by Elsevier Ltd. This is an open access article under the CC BY-NC-ND license (<http://creativecommons.org/licenses/by-nc-nd/4.0/>).

List of abbreviations

AP	arboreal pollen
CbCS	Chiba composite section
EAWM	East Asian winter monsoon
IODP	International Ocean Discovery Program/ Integrated Ocean Drilling Program
LAD	last appearance datum
MAT	Modern analogue technique
MIS	marine isotope stage
MJS	Montalbano Jonico succession
M–B boundary	Matuyama–Brunhes boundary
NIPR	National Institute of Polar Research
ODP	Ocean Drilling Program
PTI	pollen temperature index
SST	sea-surface temperature
T_{ann}	mean annual temperature
T_{inf}	Mg/Ca paleothermometry
VPDB	Vienna Pee Dee Belemnite

1. Introduction

The Earth experienced fundamental changes in oceanic and atmospheric circulation, ice sheet distributions, and biotic evolution during the transition from the Early to Middle Pleistocene (e.g., Head and Gibbard, 2005; Head et al., 2008; Head and Gibbard, 2015a). Known previously as the “mid-Pleistocene Revolution” or “mid-Pleistocene (climate) Transition” (e.g., Maasch, 1988; Mudelsee and Stettger, 1997; Mudelsee and Schulz, 1997; Raymo et al., 1997; Clark et al., 2006; Elderfield et al., 2012), it is now more properly known as the “Early–Middle Pleistocene transition” (Head and Gibbard, 2015a). A progressive increase in the amplitude of climate oscillations, the shift from a 41-ky to quasi-100 ky rhythm, increasing long-term average global ice volume, and the establishment of strong asymmetry in global ice volume cycles, all occurred during this interval (Head and Gibbard, 2015a). Significant progress has been achieved over recent decades in collecting and analyzing a wide range of climate records from terrestrial sites, marine sediment cores, and Antarctic ice cores extending back to 800 ka, and this allows us to understand how minor differences in external forcing mechanisms can lead to a wide range of responses for each glacial–interglacial cycle (e.g., Lang and Wolff, 2011; Berger et al., 2016).

The EPICA Dome C ice core record (Fig. 1a) shows that a small optimum in the δD and CO_2 signal in Marine Isotope Stage (MIS) 1 might place it within the same group of interglacials as MIS 5e, 7e,

9e, and 19c (e.g., Berger et al., 2016). Notwithstanding the influence of atmospheric CO_2 concentrations (Ganopolski et al., 2016), MIS 19 is thought to be the closest analogue for evaluating the timing, duration, and variability of the present interglacial, given the similar astronomical parameters (phasing between obliquity and precession) (e.g., Pol et al., 2010; Tzedakis, 2010; Tzedakis et al., 2012; Yin and Berger, 2012). The lowered amplitude of the 400-ky eccentricity cycle and the consequent suppression of precessional forcing are very similar for the two stages. The phasing of the obliquity maximum with the precession minimum is also similar, although obliquity increased more rapidly at the beginning of MIS 1 than of MIS 19. Detailed climatic reconstructions have revealed a cooling event at the transition from MIS 20 to MIS 19 (Termination IX) that is similar to the Younger Dryas cooling that interrupted the Last Glacial Termination (Termination I). This event appears in at least one record from the North Atlantic (IODP Site U1308; Hodell et al., 2008), at Lake Baikal (Prokopenko et al., 2006), in paleolake sediments within the Mediterranean area (Sulmona; Giaccio et al., 2015), and at the Montalbano Jonico succession (MJS) in southern Italy (Maiorano et al., 2016; Simon et al., 2017) (Fig. 1a). However, the timing, duration, and variability of the interglacial and Termination IX, including the nature of the Younger Dryas-type cooling event, are still poorly understood.

Continuous deep-ocean records across this climatic transition are common, but constructing links between atmospheric circulation, terrestrial environmental change, and biotic evolution have been hampered by the rarity of sedimentary records from near-shore areas. Therefore, continuous and highly-resolved marine records that capture both terrestrial and marine environmental signals with strong chronological controls are needed to improve our understanding of the Earth’s climate system. Geomagnetic field reversal events are additional important datums as they provide useful near-synchronous time lines that are independent of astrochronology.

The Japanese archipelago is geographically well suited for various kinds of paleoclimatic and paleoceanographic studies. Located at the easternmost margin of the Eurasian Continent and facing the Pacific Ocean, its marine sedimentary record preserves the interplay of terrestrial and marine climatic and environmental changes relating to the westerly jet, East Asian monsoon, and North Pacific Gyre (subtropical and subpolar) (Fig. 1). The Chiba composite section (CbCS), in the east-central part of the Japanese archipelago, spans most of the Pleistocene (Kazaoka et al., 2015) including a well-exposed and continuous marine sedimentary record across MIS 19. The Matuyama–Brunhes (M–B) magnetostratigraphic reversal, which is the primary chronological datum for the Lower–Middle Pleistocene Subseries boundary (Head et al., 2008), occurs immediately above a widespread tephra bed, the Ontake–Byakubi (Byk-E), in the CbCS of the Kokumoto Formation,

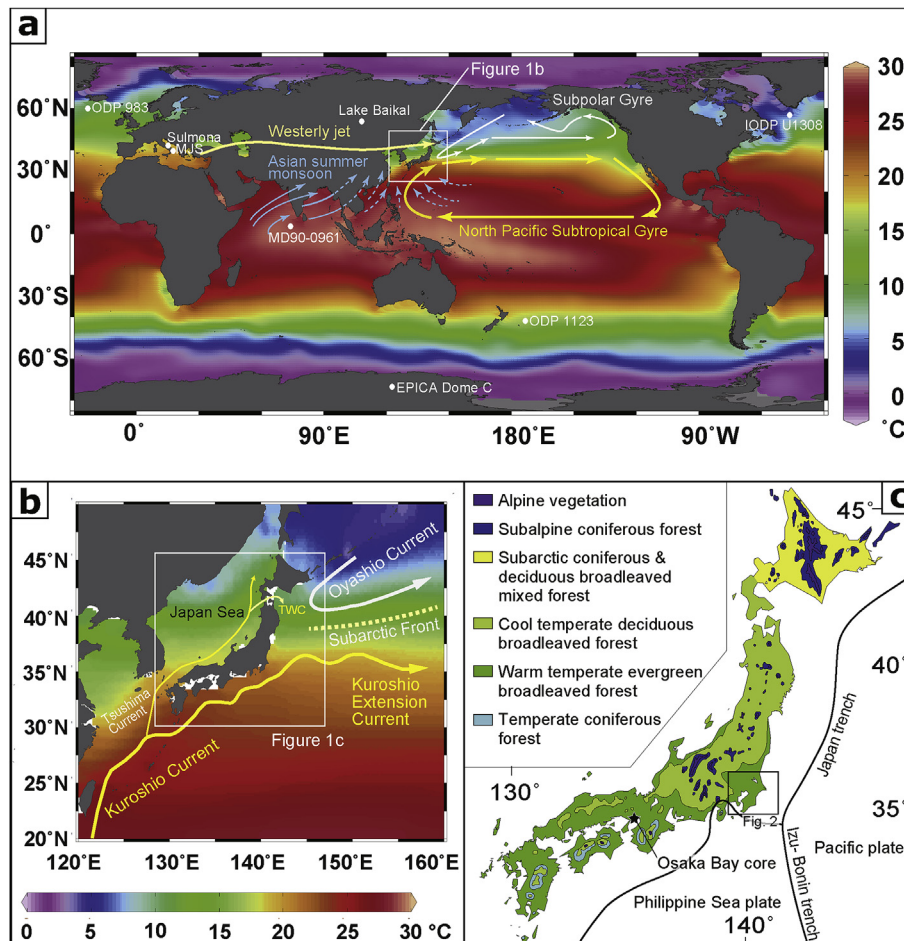


Fig. 1. The Japanese archipelago in its oceanographic, atmospheric and vegetational contexts. (a) and (b) Oceanographic and atmospheric circulation in summer. Location of the Westerly Jet is based on Zhang and Huang (2011). Positions of the major ocean currents are based on Brown et al. (2001). Ocean temperature gradients are from the World Ocean Atlas 2013 (Locarnini et al., 2013) drawn with Ocean Data View software (Schlitzer, 2015). Locations of ocean drilling sites, a lake drilling site, outcrop sections, and an Antarctic ice core are shown (see text for details). TWC = Tsugaru Warm Current; MJS = Montalbano Jonico succession. (c) Potential natural vegetation map of the Japanese archipelago simplified from Yoshioka (1973). Osaka Bay is indicated (see text for details), along with the general position of the Chiba composite section (see Figs. 2 and 3). Plate boundaries and trenches are also shown.

Kazusa Group (Suganuma et al., 2015; Hyodo et al., 2016; Okada et al., 2017). In particular, the CbCS yields well-preserved marine microfossils, pollen, paleomagnetic reversal events, and a large number of tephra beds, allowing a robust chronological and stratigraphic framework to be established.

The Boso Peninsula faces the Pacific Ocean where the subtropical Kuroshio and subarctic Oyashio currents meet just south of the Subarctic Front (Fig. 1a and b). The Kuroshio Current originates with the North Equatorial Current, flowing along the south coast of the Japanese archipelago as a part of the wind-driven subtropical gyre circulation cell. This current plays a crucial role in transporting warm and saline water towards the pole. The Oyashio Current is the western component of the Kamchatka–Alaskan Current and flows along the eastern side of the Japanese archipelago, carrying cold water towards the equator. These two currents mix in the region off the Boso Peninsula, creating the strongest latitudinal sea-surface temperature (SST) gradient in the northwestern Pacific Ocean (Fig. 1b). The variability of these two currents exerts considerable influence not only on the regional climates of East Asia but also on the global climate system (e.g., Gallagher et al., 2015).

The Subarctic Front shifted northward during the last interglacial and then southward during following glacial (Moore

et al., 1980; Thompson and Shackleton, 1980; Yamamoto et al., 2005). A Younger Dryas-type cooling event during 11–12 ka interrupted the northward shift of the Kuroshio Front during Termination 1 (Chinzei et al., 1987). This region is therefore favorable for understanding the climate dynamics of Termination I, and should be suitable for investigating older terminations including Termination IX. Evidence of Termination IX is present in the continuous and expanded sedimentary records of the CbCS.

In this paper, we construct a new high-resolution foraminiferal oxygen isotope ($\delta^{18}\text{O}$) stratigraphy for the CbCS with detailed descriptions of the tephra beds and a critical review of published data from the CbCS and surrounding region. The newly obtained geochemical paleoceanographic proxies, and marine microfossil and pollen assemblages tied to the new $\delta^{18}\text{O}$ chronology, reveal a continuous and expanded paleoclimatic and paleoceanographic record of the glacial–interglacial cycles from late MIS 20 to early MIS 18, including multi-millennial to millennial scale variations during Termination IX and the later part of MIS 19. These new studies indicate that the CbCS satisfies all stratigraphic, geochronologic and logistical requirements for defining the Lower–Middle Pleistocene Subseries boundary, including a precise and exceptional record of the M–B reversal.

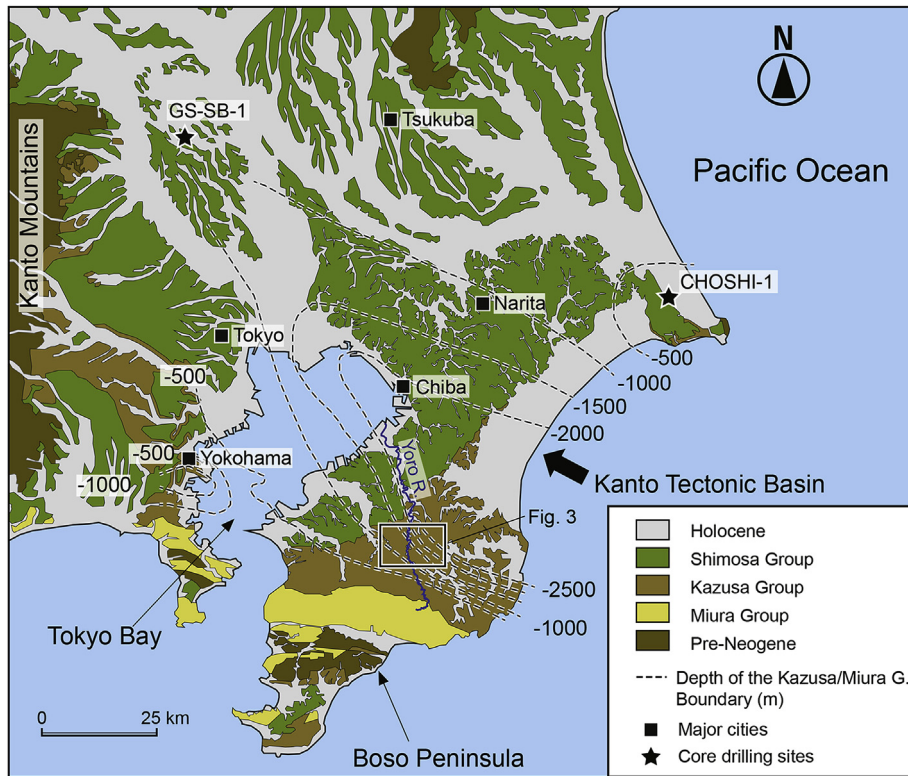


Fig. 2. Schematic geologic map of the Kanto area after Kazaoka et al. (2015). Box shows location of the geologic map in Fig. 3. The locations of deep boreholes GS-SB-1 and CHOSHI-1 are indicated. Contours show the depth (meters below sea level) of the base of the Kazusa Group (after Nirei, 1987).

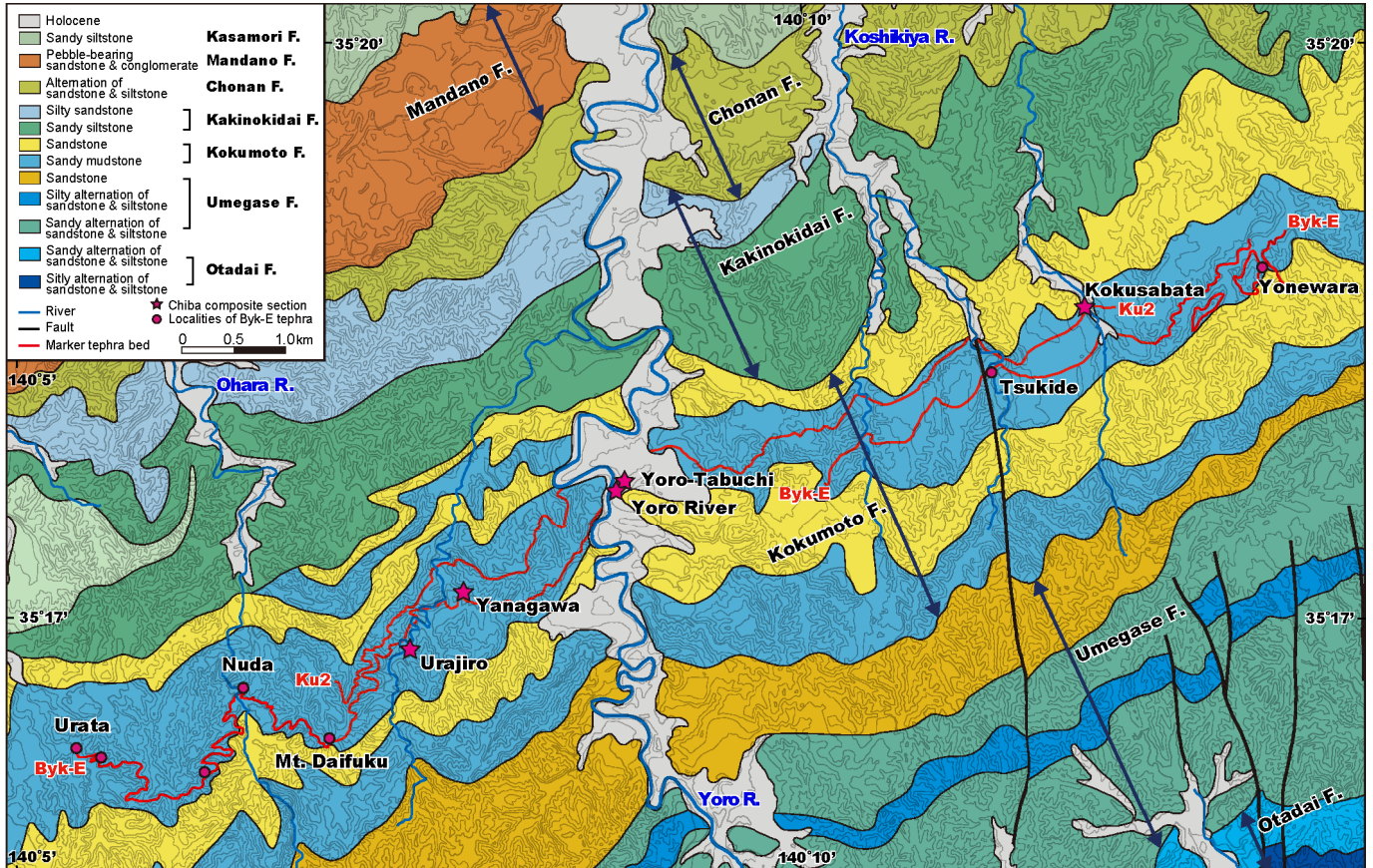
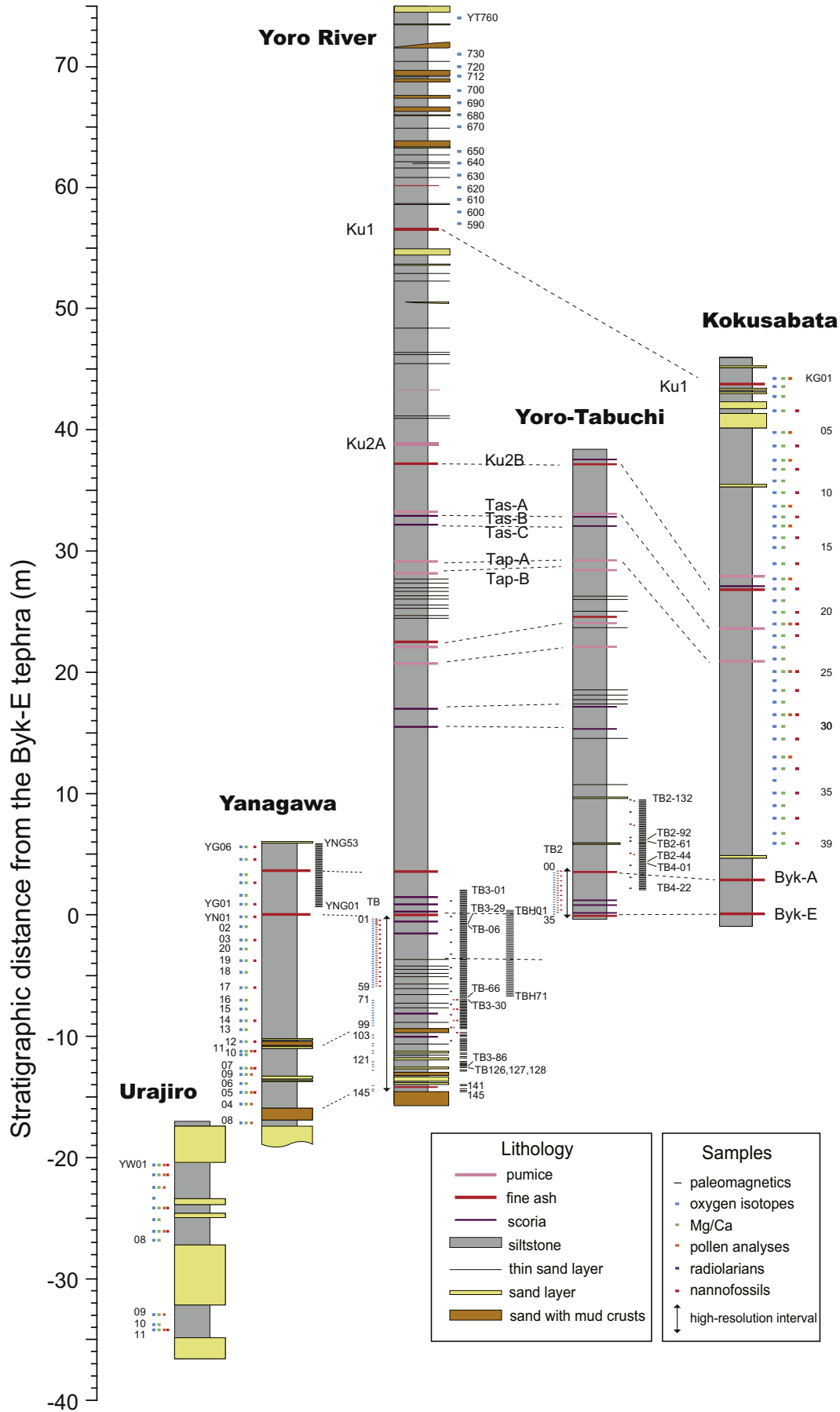


Fig. 3. Geologic map of the central part of the Boso Peninsula and location of the Chiba composite section (Yoro River, Yoro-Tabuchi, Yanagawa, Urajiro, and Kokusabata sections), modified from Mitsunashi et al. (1961) and Nirei et al. (1989). The important marker tephra beds, Ku2 and Byk-E, are shown.



2. Geological and climatic setting of the Chiba composite section (CbCS)

2.1. Geological setting

The Kazusa Group in the Boso Peninsula, southeastern part of the Chiba Prefecture, is one of the thickest (~3000 m) and best exposed Lower and Middle Pleistocene sedimentary successions in the Japanese archipelago (Ito, 1998) (Fig. 2). The Group represents the infill of the Kazusa fore-arc basin, developed in response to the west-north-westward subduction of the Pacific plate beneath the Philippine Sea plate along the Japanese archipelago and Izu-Bonin trenches (e.g., Seno and Takano, 1989), and was deposited within basin plain, submarine fan, slope, shelf, and coastal environments (Katsura, 1984; Ito and Katsura, 1992). The thickest succession (up to 3000 m) crops out continuously along the Yoro River (Fig. 3) where numerous studies based on lithostratigraphy, biostratigraphy, and paleomagnetic and $\delta^{18}\text{O}$ stratigraphy have been focused (Kazaoka et al., 2015). Well-preserved microfossils (Oda, 1977; Sato et al., 1988; Cherepanova et al., 2002) and $\delta^{18}\text{O}$ stratigraphy (Okada and Niitsuma, 1989; Pickering et al., 1999; Tsuji et al., 2005) date the Kazusa Group from 2.4 to 0.45 Ma (Ito et al., 2016).

The Kokumoto Formation, which includes the M–B boundary, occupies the middle part of the Kazusa Group (Fig. 3). It varies in thickness from 350 to 400 m and is ~350 m thick along the Yoro River (Kazaoka et al., 2015). It comprises large-scale alternations between thick silty beds and sand and thinner silt beds. Tephra beds (Ku0.1, Ku1, Ku2, Ku3, Ku5, and Ku6) provide high-resolution correlation points throughout the formation (Mitsunashi et al., 1959, 1961; Kazaoka et al., 2015).

2.2. Chiba composite section (CbCS)

2.2.1. Exposure and sections

The CbCS is a well-exposed Lower–Middle Pleistocene boundary succession within the Kokumoto Formation. This composite section comprises the Yoro River (3517.41'N; 1408.48'E), Yoro-Tabuchi (3517.41'N; 1408.49'E), Yanagawa (3517.15'N; 1407.88'E), Urajiro (3516.85'N; 1407.47'E), and Kokusabata (3518.52'N; 14011.89'E) sections (Fig. 3 and Supplementary fig. 1). These sections display the Lower–Middle Pleistocene boundary interval along deeply incised river valleys that expose the Kazusa Group (Kazaoka et al., 2015).

Exposures of the CbCS are dominated by bioturbated silts. Neither slump structures nor unconformable boundaries are present within this interval (Nishida et al., 2016). Although there are minor sands particularly in the lower part of this succession, the CbCS is generally thought to be a continuous depositional unit (Nishida et al., 2016). Nishida et al. (2016) reported paleocurrent directions from groove casts that are oriented N66E and N80E, which is consistent with the general paleocurrent directions (east to northeast) for the Kazusa Group (Ito et al., 2016).

2.2.2. Depositional environment

The Kokumoto Formation is interpreted to be a shelf edge to continental slope deposit (Ito, 1992; Ito and Katsura, 1992; Ito et al.,

2006a; b; Nakamura et al., 2007). The trace fossil assemblages in the formation also support this interpretation (Nishida et al., 2016). The ichnogenera of the silty beds of the Yoro-Tabuchi section are typical of deep-sea siliciclastic systems (Hubbard et al., 2012; Uchman and Wetzel, 2012; Wetzel and Uchman, 2012), and the trace fossil assemblages of the Yoro River section are similar to the deep-water Pleistocene sediments at IODP Site U1385 (the Shackleton Site) on the continental slope of the southwestern Iberian margin (Hodell et al., 2013; Rodríguez-Tovar and Dorador, 2014).

A seismic profile across Tokyo Bay shows that a depositional unit correlated with the Kokumoto Formation onlaps an inclined surface (Chiba Prefecture, 2004; Kazaoka et al., 2015), which is consistent with the interpretation that the Kokumoto Formation was deposited on a stable continental slope (Kazaoka et al., 2015). Kamemaru (1996) interpreted a water depth of less than 200 m for the Kokumoto Formation based on benthic foraminiferal assemblages with sublittoral taxa including *Elphidium* spp., *Cibicides* spp. and *Pseudonion japonicum*. However, the bathyal species *Bulimina aculeata*, *Melonis parkerae* and *Bolivinita quadrilatera* are also present (Itihara et al., 1973; Igarashi and Kamemaru, 2011), suggesting that the paleodepths were greater than 200 m, and that reworking accounts for the sublittoral species (Kazaoka et al., 2015).

2.2.3. Macrofossil and microfossil records

A number of biostratigraphic studies of macrofossils and microfossils have been carried out on the Kazusa Group. Microfossils have been used to age constrain the formations in the Kazusa Group and to estimate changes in oceanic environments around the Pacific margin of east-central Japan during the Pleistocene (see Kazaoka et al., 2015 for details). The age of the Kokumoto Formation is placed between the last appearance datum (LAD) of the calcareous nannofossil *Reticulofenestra asanoi* (0.889 ± 0.025 Ma in the Ontong Java Plateau; Berger et al., 1994) and the LAD of *Pseudoemiliana lacunosa* (0.433 ± 0.020 Ma in the Ontong Java Plateau; Berger et al., 1994; Sato et al., 1988). However, while these datums constrain the succession below and above the Kokumoto Formation, no calcareous nannofossil biohorizons have been documented within the formation itself. Some important planktonic foraminiferal and diatom datums have been identified (Oda, 1977; Cherepanova et al., 2002). Igarashi (1996) suggested that the co-occurrences of *Globorotalia truncatulinoides* and *Globorotalia tosaensis* in the Kokumoto Formation have an N22 zonal age of Blow (1969). The biostratigraphic configurations are also supported by the highest occurrences of two diatom species, *Proboscia curvirostris* and *Nitzschia fossilis*, in the upper part of the Kokumoto Formation (Cherepanova et al., 2002).

Planktonic foraminiferal assemblages of the Kokumoto Formation suggest that the Subarctic Front between the subtropical Kuroshio and subarctic Oyashio currents shifted northward just after the M–B boundary (Igarashi, 1994). Benthic foraminiferal assemblages have been used to evaluate depositional environments within the Kazusa Group (Itihara et al., 1973).

Terrestrial climates during the deposition of the Kazusa Group were reconstructed by Onishi (1969) based on pollen assemblages. Dominant occurrences of *Pinus*, *Picea*, *Tsuga*, and *Taxodiaceae* (*Metasequoia*, *Cryptomeria*, etc.) with minor broad-leaved trees and herbs were observed. Onishi (1969) also reported that the

Fig. 4. Sampling horizons for the Chiba composite section (CbCS). Detailed stratigraphic correlations between the Urajiro, Yanagawa, Yoro River, Yoro-Tabuchi, and Kokusabata sections, based on lithological changes and marker tephra beds, are given. The stratigraphic correlations are revised from Okada et al. (2017) to provide more detailed information about each section. Samples for paleomagnetic (thin black horizontal lines), $\delta^{18}\text{O}$ (light blue rectangles), and Mg/Ca (green rectangles) measurements including previous studies (Suganuma et al., 2015; Okada et al., 2017), and analyses of pollen (orange rectangles) and marine microfossils (calcareous nannofossil: red rectangles and radiolarians: purple rectangles), are shown. The black arrows show high resolution sampling intervals (0.2 m spacing) for oxygen isotope analyses. (For interpretation of the references to colour in this figure legend, the reader is referred to the Web version of this article.)

disappearance of *Metasequoia*, a component of the northern Hemisphere flora from the Late Cretaceous to Quaternary, occurs in the middle of the Kokumoto Formation.

2.2.4. Tephrostratigraphy

2.2.4.1. Byk-E tephra. Formally known as the Ontake-Byakubi tephra (Takeshita et al., 2016), the Byk-E is a widely distributed tephra in the central part of the Boso Peninsula (Okada and Niitsuma, 1989; Kazaoka et al., 2015; Nanayama et al., 2016). It is a white pumiceous fine ash deposit 1–7 cm thick, interbedded with dark gray sandy silt units (or layers) in the middle of the Kokumoto Formation. The Byk-E tephra is mainly composed of pumice-type glass shards, and contains abundant hornblende and small amounts of orthopyroxene and clinopyroxene. The range in refractive indices of the volcanic glass shards and hornblende grains are 1.505–1.510 and 1.680–1.703, respectively (Nishida et al., 2016; Nanayama et al., 2016). Based on lithofacies, bulk grain composition, mafic mineral composition, major element composition of hornblende, and stratigraphic relationships, the Byk-E tephra is correlated with the YUT5 bed erupted from the Older Ontake volcano in the central part of the Japanese archipelago (Takeshita et al., 2016). Sugauma et al. (2015) dated the Byk-E tephra to 772.7 ± 7.2 ka using U-Pb zircon ages.

2.2.4.2. Other tephtras. Several minor tephtra beds are present in the CbCS (Kazaoka et al., 2015; Nishida et al., 2016). Byk is a series of five individual tephtra units, including the Byk-E tephtra mentioned above. Byk-D, -C, and -B tephtras, in ascending order, are lenticular beds of medium-sand-sized scoria 1–5 cm thick, interbedded with silt, 0.2 m, 0.8 m, and 1.4 m above the Byk-E tephtra. The Byk-A tephtra, a 9-cm-thick bed of reddish-gray vitric fine ash, is interbedded with silt, 3.6 m above the Byk-E tephtra (Nishida et al., 2016).

The Tap and Tas tephtras are in thick and massive siltstones in the upper part of the CbCS (Kazaoka et al., 2015). The Tap tephtra comprises two layers (Tap-B and Tap-A), and the Tas tephtra comprises three layers (Tas-C, -B, and -A) (Nishida et al., 2016). The Tap-A tephtra and Tas-A tephtra lie at about 8.9 and 5.1 m below the Ku2A tephtra, respectively (Fig. 4).

The well documented and widespread tephtra beds Ku2 and Ku1 are present within the CbCS (Kazaoka et al., 2015). The Ku2 consists of two tephtra beds, Ku2B and Ku2A. The Ku2B tephtra has a thickness of about 6 cm, and is subdivided into three units in ascending order: 1) reddish brown fine ash with white coarse-sand-sized pumice, 2) black, medium-sand-sized scoriaceous tephtra, and 3) reddish brown silt-sized tephtra (Satoguchi, 1995). The Ku2A tephtra is a 6–9 cm thick, white medium sand to 30-mm sized pumiceous ash. The Ku1 tephtra lies 15 m above the Ku2A tephtra. It is ~25 cm thick, varies from gray to white, and has normal grading from very fine sand to silt-sized ash. The Ku2 and Ku1 tephtras have been correlated to the Yk8.5 and Yk9a tephtras respectively in the CHOSHI-1 sediment core at the city of Choshi in the easternmost part of the Boso Peninsula (Fig. 2) (Nakazato et al., 2003). The Ku1 tephtra correlates with the Hakkoda-Kokumoto (Hkd-Ku) tephtra in the central to northern parts of the main island of Japan (Suzuki et al., 2005).

2.2.5. Magneto- and oxygen isotope ($\delta^{18}\text{O}$) stratigraphy

The M–B boundary occurs in the middle of the CbCS within the Kokumoto Formation (Niitsuma, 1976; Okada and Niitsuma, 1989; Aida, 1997; Tsunakawa et al., 1999; Sugauma et al., 2015). This boundary was originally considered to be 1–2 m below the Byk-E tephtra (Niitsuma, 1976; Okada and Niitsuma, 1989; Tsunakawa et al., 1999), but Sugauma et al. (2015) using thermal demagnetization located it at ~0.8 m above the Byk-E tephtra in the Yanagawa

section.

Recently, Okada et al. (2017) described a detailed virtual geomagnetic pole (VGP) path from the Yoro-Tabuchi section at 10-cm resolution across the M–B boundary. Although the VGP record shows several subsequent rebounds, Okada et al. (2017) defined the zone between 0.25 m and 1.95 m as the directional transition zone of the M–B boundary, and reported the actual boundary at 1.1 m above the Byk-E tephtra in the Yoro-Tabuchi section. The horizon of the M–B boundary is nearly consistent with that shown in a drilled core from the vicinity of this section (Hyodo et al., 2016) and in the Yanagawa section (Sugauma et al., 2015) (Fig. 4).

A $\delta^{18}\text{O}$ stratigraphy for the Kazusa Group, including the CbCS, was conducted by Okada and Niitsuma (1989) and Pickering et al. (1999). MIS 35 to MIS 15 and substages within MIS 21–16 were identified using graphical correlation to astronomically tuned isotope records. In the CbCS, the strata are assigned to MIS 21 to MIS 18 (Okada and Niitsuma, 1989; Pickering et al., 1999), with glacial–interglacial cycles corresponding respectively to sandstone–siltstone-dominated units. More recently, Sugauma et al. (2015) and Okada et al. (2017) constructed a detailed $\delta^{18}\text{O}$ stratigraphy for the CbCS for the interval from late MIS 20 to early MIS 18.

2.3. Present oceanographic conditions of the northwestern Pacific Ocean and climate of the southeastern Japanese archipelago

The Boso Peninsula is situated in the east-central part of the Japanese archipelago, facing the Pacific Ocean (Fig. 1a and b). The northwestern Pacific Ocean contains the Subarctic Front between the subtropical Kuroshio and subarctic Oyashio currents (Fig. 1b). The Oyashio Current sinks beneath the Kuroshio Current at the Subarctic Front (Supplementary fig. 3b and c). The annual mean SST of the Oyashio Current off the northern part of the Japanese archipelago is 4–8 °C, whereas the Kuroshio Current SST off central Japan is 20–22 °C (Fig. 1b). Similarly, a sea-surface salinity gradient is present between Oyashio- (~33.0) and Kuroshio-influenced regions (~34.5) (Supplementary fig. 3a). The Kuroshio Current is oligotrophic, whereas the Oyashio Current is nutrient-rich. The interplay between these two current systems accordingly has a profound impact on the marine biota (Gallagher et al., 2015).

Mountain ranges up to ~3000 m are present in the central part of the Japanese archipelago, west and north of the Boso Peninsula (Fig. 1c). The summer (June–September) rainfall and mean temperature of Chiba City from 1981 to 2010 were 607 mm and 24.1 °C, with 1387 mm and 15.7 °C for the annual rainfall and mean temperature (Japan Meteorological Agency). The present natural vegetation of the Kanto Basin is mainly warm-temperate broad-leaved evergreen forest. Cool-temperate deciduous broadleaved and coniferous forests characterize the surrounding higher-relief ranges of the Kanto Basin as well as the northern part of the main island of Japan (Fig. 1c; Yoshioka, 1973).

3. An improved age model for the Chiba composite section (CbCS)

In this study, we construct a new $\delta^{18}\text{O}$ stratigraphy for the CbCS based on benthic foraminiferal species from the sample set of Okada et al. (2017) and Sugauma et al. (2015), and newly obtained samples from the upper part of the Yoro River section (Fig. 4). In the age models of Sugauma et al. (2015) and Okada et al. (2017), the MIS 19–18 boundary within the CbCS was determined by correlating to the much longer $\delta^{18}\text{O}$ record obtained from the CHOSHI-1 core (Kameo et al., 2006). This correlation was based on a visual correlation of the $\delta^{18}\text{O}$ records supported by the stratigraphic positions of the Ku1 and Ku2 tephtras (Fig. 5). Our new $\delta^{18}\text{O}$ stratigraphy enables us to locate the MIS 19–18 boundary directly,

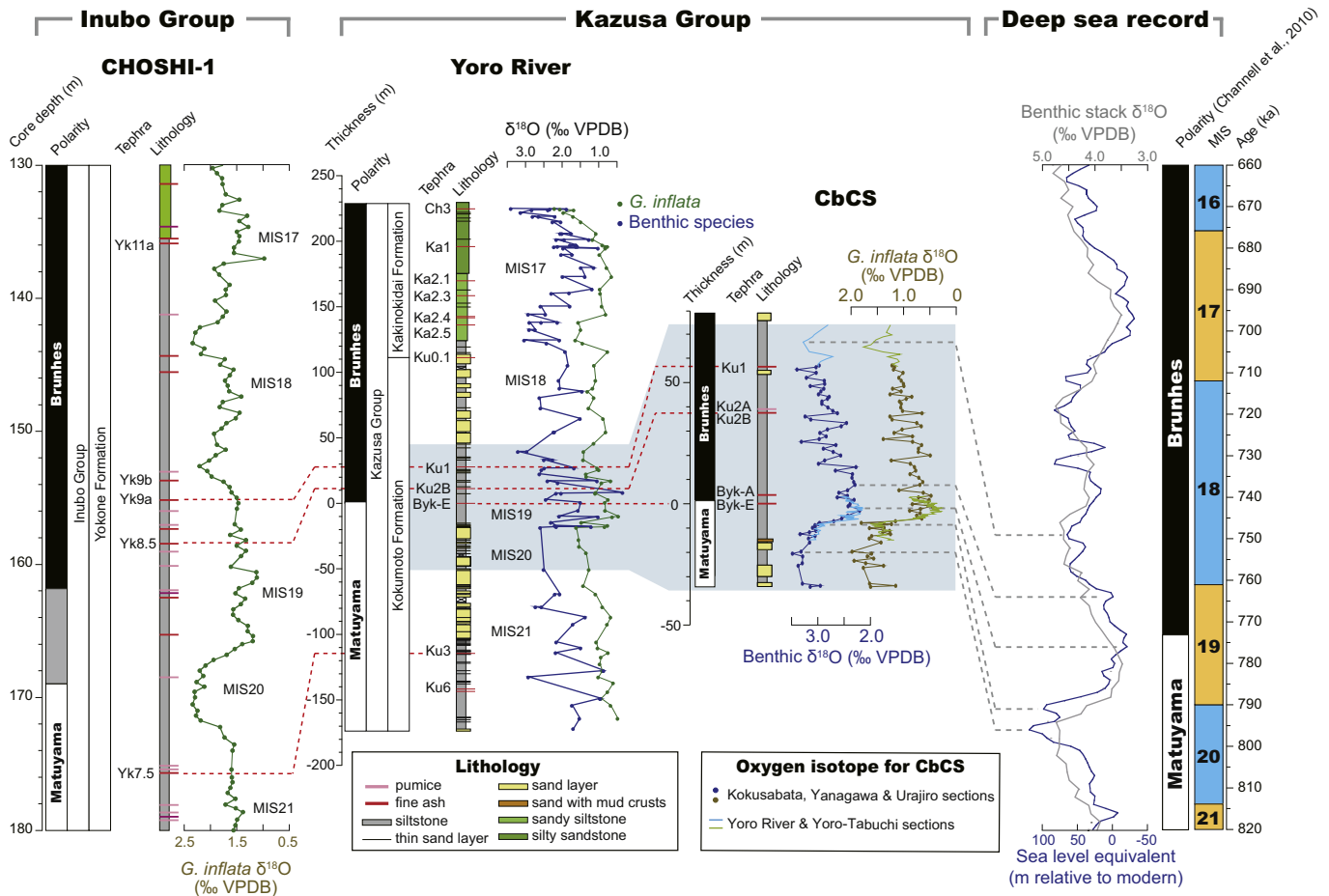


Fig. 5. Chronostratigraphic correlations between the Kazusa Group, including the Chiba composite section (CbCS), and the Inubo Group. The CHOSHI-1 core is thought to recover the homogeneous hemipelagic silt/clay sediments of the Inubo Group (Ozaki, 1958; El-Masry et al., 2002), and the age model is based on visual matching with the sea level proxy of Elderfield et al. (2012). The LR04 benthic stack (Lisiecki and Raymo, 2005) is also shown for comparison. VPDB: Vienna Pee Dee Belemnite, MIS: Marine Isotope Stage. The ages of the MIS boundaries follow Lisiecki and Raymo (2005) and are taken from http://www.lorraine-lisiecki.com/LR04_MISboundaries.txt. To refine marker tephra correlation, we have newly measured major elemental compositions of the volcanic glass shards from these tephra beds (Supplementary table 1 and fig. 2). Our data show that the major elemental compositions of Ku1 and Ku2B are similar those of Yk9a and Yk8.5, confirming this correlation.

resulting in a more reliable age model for the CbCS.

Our new age model for the CbCS is established by correlating to the sea level proxy curve of Ocean Drilling Program (ODP) Site 1123 (Elderfield et al., 2012) (Fig. 6). Because the sea level proxy curve was constructed by subtracting the effects of deep-water temperature on the $\delta^{18}\text{O}$ record, this is an ideal target to establish an age model. Based on benthic foraminiferal $\delta^{18}\text{O}$ trends, we assign substages to MIS 19 using the nomenclature of Railsback et al. (2015) (Fig. 6). Astronomical ages for each of the substage boundaries are estimated to be 771.7 ka (MIS 19c–19b) and 766.6 ka (MIS 19b–19a).

Sedimentation rates in the section generally decrease during sea-level highstand periods, and increase during lowstands (Fig. 6). The M–B boundary is in an interval with sedimentation rates of 89 cm/kyr, which is low compared with other intervals in the CbCS but high enough to minimize PDRM lock-in (Suganuma et al., 2010, 2011).

Okada et al. (2017) have shown that the mid-horizon of the directional transition zone, assigned as the M–B boundary, is 1.1 m above the Byk-E tephra. Our $\delta^{18}\text{O}$ stratigraphy indicates that the M–B boundary has an astronomical age of 772.9 ka, with a duration of 1.9 kyr for the directional transition. This age is consistent with a recalculated radiometric age for the M–B boundary of 771.7 ± 7.3 ka using the U–Pb zircon age of Suganuma et al. (2015) and the new $\delta^{18}\text{O}$ chronology.

4. Procedures of paleontological and geochemical analyses

4.1. Pollen analyses

The pollen assemblages were analyzed to determine paleoclimatic and paleoenvironmental changes from late MIS 20 to early MIS 18 based on 98 samples from the CbCS (Fig. 4, Supplementary table 2 and fig. 4). The weight of sediment sample for each pollen analysis was <2 g. The average pollen concentration for the samples is 2244 grains/g (with a range from 414 to 6266 grains/g), which is higher than typical for sediments deposited in open marine environments.

Samples were subjected to a 10% potassium hydroxide treatment, followed by sieving (to obtain a 1–250 μm fraction) and decanting partly using a swirling technique. After hydrofluoric acid treatment, the organic fraction including pollen was then concentrated using heavy liquid separation with a zinc chloride solution (density 1.998–2.002). Acetolysis treatment followed, and without further sieving the residues were mounted on microscope slides using glycerine jelly. Fossil pollen grains were identified under a light microscope at 400 \times or 600 \times magnification. At least 200 grains of trees and shrubs were counted in each sample. Pollen grains of herbs and spores of pteridophytes were also identified and counted. Some typical pollen types obtained from the CbCS are

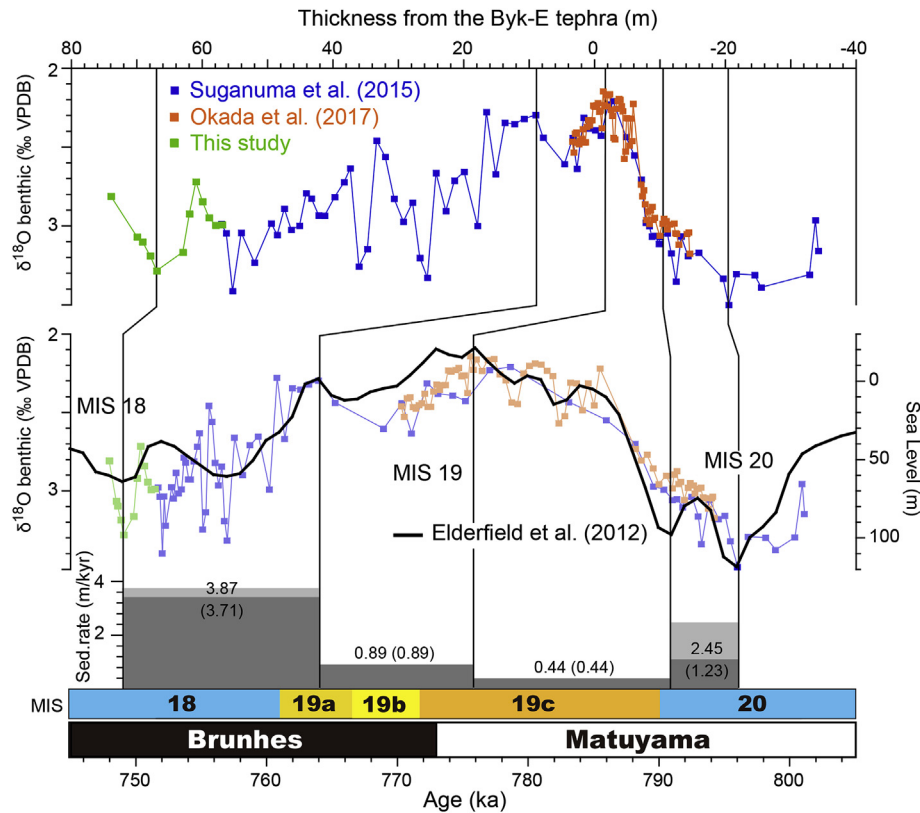


Fig. 6. Age–depth model based on the high-resolution $\delta^{18}\text{O}$ stratigraphy from the Chiba composite section (CbCS). The $\delta^{18}\text{O}$ stratigraphy, combined with those of Suganuma et al. (2015) (blue squares) and Okada et al. (2017) (orange squares), is visually tuned to the eustatic curve of Elderfield et al. (2012) using major features of the $\delta^{18}\text{O}$ record, with assistance from the U–Pb age of the Byk–E tephra. The M–B boundary age is estimated at 772.9 ka based on this age model. Sedimentation rates for the section with (light gray bars) and without (dark gray bars) the sandstone (no sandstones during MIS 19). VPDB: Vienna Pee Dee Belemnite, MIS: marine isotope stage. (For interpretation of the references to colour in this figure legend, the reader is referred to the Web version of this article.)

shown in Supplementary fig. 5.

Quantitative paleotemperature reconstruction was carried out by applying the modern analogue technique (MAT) (Nakagawa et al., 2002) using Polygon 2.4.4 software based on a surface pollen dataset covering the Japanese archipelago (Gotanda et al., 2002). *Pinus* is excluded from both fossil and surface pollen datasets for the MAT calculation because of the exotic nature of *Pinus* as described below.

4.2. Marine microfossils

In this study, we analyzed planktonic foraminifera, calcareous nannofossils and radiolarians for the paleoceanographic interpretation of the CbCS. We reexamined Igarashi's (1996) samples (Supplementary table 3) to investigate planktonic foraminiferal assemblages in addition to Igarashi's (1994) data. In total, 33 samples from the Kokumoto Formation were analyzed (Supplementary fig. 6). Each sample was disaggregated using standard procedures including sodium sulfate and naphtha solutions (Igarashi, 1994, 1996). More than 300 tests of planktonic foraminifera were picked from the $>125\ \mu\text{m}$ fraction of each sample and identified under a binocular microscope. The published data set from the Kokumoto Formation (Igarashi, 1994) was also used for the faunal analysis.

Calcareous nannofossils in 63 samples from the CbCS were examined (Supplementary table 4 and fig. 7). Smear slides were prepared and a counting technique was applied to distinguish the overall assemblages throughout the sections. For each sample, 200 specimens were counted, followed by a search for rare species.

Nannofossils were documented using a binocular polarizing microscope (Olympus BX51) at $1500\times$ magnification.

For radiolarian analysis, 44 samples were used (Supplementary table 5). Samples were dried, weighed, and then wet sieved using a $45\ \mu\text{m}$ mesh, after which two types of slides were made to quantify the abundance and faunal analysis based on the standard technique described in Itaki et al. (2009). Relative abundances (% of total assemblage) of species were estimated by identifying and counting more than 200 individuals on a slide, although when radiolarians were rare, as many as possible were counted.

4.3. Foraminiferal geochemistry

We analyzed foraminiferal $\delta^{18}\text{O}$ from the CbCS not only for benthic species but also the planktonic species *Globigerina bulloides* and *Globorotalia inflata*. These samples were disaggregated primarily using the sodium sulfate method and partly using a SELFRAG high voltage pulse fragmentation system installed at the National Institute of Polar Research (NIPR). The non-magnetic fraction including foraminifera was concentrated using an isodynamic separator at Ibaraki University. We manually picked foraminiferal tests from the non-magnetic fraction for each sample. $\delta^{18}\text{O}$ measurements were taken using a Finnigan–MAT253 isotope mass spectrometer coupled with a Kiel IV carbonate preparation device installed at the Department of Geology and Paleontology, National Museum of Nature and Science, and a GV instruments IsoPrime with the Multicarb preparation system installed at the Center for Advanced Marine Research, Kochi University. JcP-1, CO-1, and NBS-19 were used as standards to calibrate the measured isotopic values

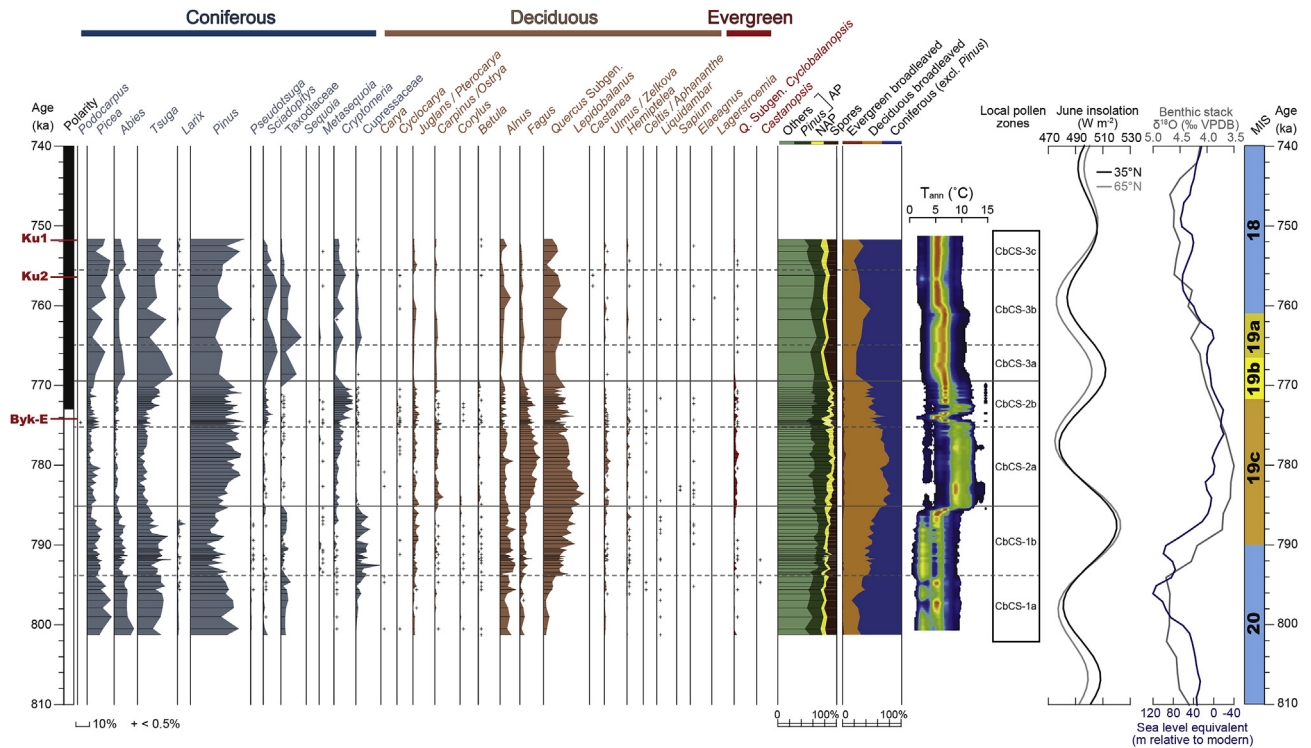


Fig. 7. Percentage pollen diagram for the Chiba composite section (CbCS). The pollen sum for percentage calculations consists of the total arboreal pollen (AP) including *Pinus*, with non-arboreal pollen (NAP) and pteridophyte and bryophyte spores excluded. Cumulative frequencies of AP, NAP and spores are also summarized. The arboreal pollen is further subdivided into evergreen broadleaved trees, deciduous broadleaved trees and coniferous trees (excluding *Pinus*), with the ratio between the combined broadleaved pollen and the total tree pollen excluding *Pinus* (“broadleaved/AP”) employed as a substitutional temperature proxy. Quantified variations in the mean annual temperature (T_{ann}) is based on the modern analogue technique (Nakagawa et al., 2002), converted from the fossil pollen spectra using the modern surface pollen dataset covering the Japanese archipelago (Gotanda et al., 2002). The LR04 benthic stack (Lisiecki and Raymo, 2005), the eustatic curve of Elderfield et al. (2012), and the 65N and 35N June insolation curves are shown for comparison.

to the Vienna Pee Dee Belemnite (VPDB). The standard deviation of the $\delta^{18}\text{O}$ measurements was calculated as 0.049‰ from 148 measurements of NBS-19 working standard specimens. We used more than 20 individuals of *G. inflata* with a test size greater than 250 μm diameter for each isotopic measurement. For *G. bulloides*, we used >250 μm size interval for the Yanagawa, Urajiro, and Kokusabata sections, and 150–250 μm size interval for Yoro River and Yoro-Tabuchi sections. Most measurements on *G. bulloides* were based on 20 individuals or more, but a few measurements used fewer than 20 individuals where abundances of this species were low.

Mg/Ca analysis was carried out on 74 samples from 73 sampling intervals (with two samples from one sampling interval) used for the $\delta^{18}\text{O}$ from the CbCS (Fig. 4). Approximately 20 individuals of *G. inflata* from the size fraction >250 μm were analyzed. The samples were cleaned using the “reductive” cleaning protocols of Boyle and Keigwin (1987) with slight modification (Kubota et al., 2010). Mg/Ca analysis was performed using a Finnigan ELEMENT XR sector-field inductively coupled plasma mass spectrometer at the Mutsu Institute for Oceanography (MIO), JAMSTEC. Isotopes of three elements (^{24}Mg , ^{44}Ca , ^{48}Ca , and ^{55}Mn) were analyzed using Sc as the internal standard (Uchida et al., 2008). The relative standard deviation of Mg/Ca for the replicate measurement of a standard solution was less than 3%.

5. Results

5.1. Vegetational and climatic reconstructions

The pollen assemblages reveal an excellent record of the regional climate and environmental variability from late MIS 20 to

early MIS 18 that is consistent with the global glacial–interglacial climate pattern (Fig. 7). The glacial MIS 20 and MIS 18 are dominated by the boreal conifers *Picea*, *Abies*, and *Tsuga*, whereas the interglacial MIS 19 is marked by broadleaved trees including *Quercus* (subgenus *Lepidobalanus*, hereafter *Quercus*), *Fagus*, *Ulmus*/*Zelkova* and *Carpinus*/*Ostrya*. Although *Pinus* pollen is dominant throughout the section, it is often overrepresented in deep-sea sediments because of its buoyant character (Heusser, 1990; Okuda et al., 2006) and so we omit *Pinus* from our interpretation. The occurrence of *Metasequoia*, an extant coniferous tree that disappeared from Japan by the latest Early Pleistocene (Tai, 1973; LePage et al., 2005; Momohara, 2005), is largely consistent with our age model, although it is rare and sporadic throughout our record. Our palynoflora is mostly represented by tree pollen (80–90% in total), with no herb pollen or embryophyte spores exceeding 10–20%. Based on the alternation between boreal conifer and temperate broadleaved trees, our pollen record is divided into three palynological assemblage zones, CbCS-1 to -3, in ascending order.

Zone CbCS-1 (801.1–785.0 ka) is dominated by the boreal conifers *Picea*, *Abies* and *Tsuga*. The percentage of broadleaved trees with respect to the total AP (arboreal pollen excluding *Pinus*) ranges from 20 to 55%, so the reconstructed vegetation is a subarctic coniferous and deciduous broadleaved mixed forest, which is today prevalent between 42°N and 45°N in Japan (see Fig. 1c). The paleotemperature based on the MAT is 2–8 °C (mean annual temperature). Zone CbCS-1 represents MIS 20 to early MIS 19. It is subdivided into subzone CbCS-1a which reflects the full glacial conditions of MIS 20, and CbCS-1b which spans the transition from MIS 20 to MIS 19 and is based on the higher values of *Quercus* and *Fagus*.

Zone CbCS-2 (785.0–769.3 ka) is characterized by abundant *Quercus* and *Fagus*. Boreal conifers (*Picea*, *Abies* and *Tsuga*) decrease, and other deciduous broadleaved trees (*Carpinus*/*Ostrya*, etc.) occur regularly. The ratio of broadleaved trees to the total AP excluding *Pinus* is > 40–80%, and therefore the reconstructed vegetation of zone CbCS-2 is cool-temperate deciduous broadleaved forest, which is today seen between 35°N and 42°N in Japan (Fig. 1c). The estimated paleotemperature based on the MAT is 4–12 °C (mean annual temperature). The upper part of zone CbCS-2 is differentiated as subzone CbCS-2b based on the higher values of temperate conifers (*Cryptomeria*, *Sciadopitys*, etc.), possibly reflecting gradual cooling during MIS 19b. Thus, subzone CbCS-2a is thought to represent full interglacial conditions and occurs within MIS 19c. There appears to be a short temperature anomaly at ~774 ka based on the MAT. Because of the absence of significant changes in pollen composition around 774 ka, we consider that the temperature anomaly is overestimated due to the heterogeneous temporal resolution of our data.

Zone CbCS-3 (769.3–751.6 ka) is dominated by boreal conifers (*Picea*, *Abies* and *Tsuga*) at the expense of broadleaved trees except *Quercus*. Although the ratio of broadleaved pollen to the total AP decreases to 20–40%, zone CbCS-3 differs from zone CbCS-1 in the persistence of temperate conifers (*Cryptomeria*, etc.). The estimated paleotemperature for CbCS-3 based on the MAT is 4–7 °C. The intermediate character of zone CbCS-3 reflects that fact that it extends from the middle of MIS 19b into early MIS 18. The slight warming observed at ~761–763 ka may represent the interstadial phase of MIS 19a.

5.2. Marine microfossils

5.2.1. Planktonic foraminifera

A total of 37 species belonging to 11 genera of planktonic foraminifera are recognized from 12 samples of Igarashi's (1996) study (Supplementary table 3). Preservation is generally good to excellent with very slight fragmentation. No weathering of the test surfaces, nor secondary calcification, were observed. The fauna in the CbCS can be divided into two intervals with their boundary at 3–4 m above the Byk-E tephra (~770 ka). The lower interval is dominated by *Neogloboquadrina incompta* (20–50%) and the dextral form of *Neogloboquadrina pachyderma* (15–30%). Above this level, these two species are rare (3–10%) whereas *Globorotalia inflata* is common to abundant (~10–50%). *N. incompta* presently flourishes in highly stratified water near the Subarctic Front (Schiebel et al., 2001; Kuroyanagi and Kawahata, 2004). This species is presently an indicator of the Tsugaru Warm Current (Oda et al., 1983) because it dominates in the Japan Sea owing to the highly stratified conditions there (Fig. 1). The dextral form of *N. pachyderma* is also the main component of the mixed water region near the Subarctic Front (Kuroyanagi and Kawahata, 2004). In contrast, *G. inflata* typifies the central water mass near the northern margin of the Kuroshio Current (Vincent and Berger, 1981). Igarashi (1996) noted that changes in the proportions of these three species at the CbCS reflect the three major current systems, namely the Oyashio and Kuroshio currents, and Tsugaru Warm Current (Fig. 1b).

In this study, we calculated the varimax factor loadings and regional transfer function of PFJ-125 (Takemoto and Oda, 1997), following the methodology of Imbrie and Kipp (1971), for the Kokumoto Formation assemblages to interpret the paleoceanographic settings near the M–B boundary. PFJ-125 equations yield winter and summer SSTs with standard errors of 1.75 °C and 1.17 °C. Niimura et al. (2006) extended the equations to give the annual mean SST with a standard error of 1.35 °C. Calculated varimax factor loadings and reconstructed SSTs using PFJ-125 are shown in Fig. 8, and Supplementary table 6 and fig. 6. Results of the factor analysis

show high loadings (0.48–0.89) for the second factor in most of the studied interval, indicating an influence of transitional water masses. The first factor loading (Kuroshio components) is generally significant (>0.5) after ~770 ka, whereas quite low values occur for the lower horizons. The reconstructed annual mean SST ranges from 16.8 to 21.5 °C and shows a sudden increase of ~4 °C that coincides with the faunal change at ~770 ka. Correlating with the modern surface sediments based on squared chord distance, the oceanographic settings across the faunal change might compare with a shift from the region of the Tsugaru Warm Current (sample MkuY-280) to that of the Kuroshio Current with subsurface cold water originating from the Oyashio Current (sample MkuY-280) (Supplementary figs. 3 and 6).

5.2.2. Calcareous nannofossils

At least 15 genera and 17 species of calcareous nannofossils have been identified (Fig. 10 and Supplementary table 4) based on preliminary results presented by Kameo et al. (2016, 2017), with the addition of new assemblage data in the present study. The dominant taxa are *Gephyrocapsa* spp., including *Gephyrocapsa omega*, *Gephyrocapsa oceanica*, and other smaller *Gephyrocapsa* specimens. We classified the *Gephyrocapsa* specimens into small-sized *Gephyrocapsa* (<4 µm in diameter) and medium-sized *Gephyrocapsa* (≥4 µm in diameter) based on the size of the major axis of an individual coccolith. *Gephyrocapsa* specimens comprised almost 40%–90% of the total flora with a 70% average. Specimens of *Gephyrocapsa* exceeding 4 µm and with a bridge aligned near the minor axis are present throughout the section. They possibly correspond to *Gephyrocapsa omega*, *Gephyrocapsa* sp. 3 of Rio et al. (1982), and *Gephyrocapsa* sp. C, and/or *Gephyrocapsa* sp. D of Matsuoka and Okada (1990). *Florisphaera profunda*, a lower photic zone species in the low to middle latitudes (Okada and Honjo, 1973), is abundant especially from 787.5 ka (~6–15% of the total flora). *Pseudoemiliana lacunosa*, *Umbilicosphaera sibogae*, and *Calcidiscus leptoporus* were recorded with abundances of a few percent (Fig. 10 and Supplementary fig. 7). Two subspecies of *Coccolithus pelagicus* are present: *Coccolithus pelagicus braarudii*, an upwelling subspecies in the North Atlantic Ocean (Parente et al., 2004), is more abundant than the cold-water subspecies *Coccolithus pelagicus pelagicus* especially from 772 ka onwards.

5.2.3. Radiolarians

The total radiolarian concentrations range between 80 and 1300 individuals/g, and show higher values during the peak of MIS 19c. More than 36 species and species groups have been recorded (Motoyama et al., 2017). Relative abundance changes of major radiolarian groups are shown in Supplementary table 5 and fig. 8.

Radiolarian assemblages are characterized by warm water species including *Dictyocoryne* spp., *Didymocorytis* spp. and *Tetrapyle* spp., especially during MIS 19 in the CbCS. At present, higher abundances of these groups occur in the Kuroshio Current where sea-surface temperatures range between 20 and 29 °C (Matsuzaki and Itaki, 2017). However, *Lithomelissa setosa* is related to cold waters ranging between 12 and 18 °C (Matsuzaki and Itaki, 2017) and tends to increase in abundance when warm water species decrease. *Stylochlamydidium venustum* predominates in the Oyashio Current today (e.g., Kruglikova, 1969). Although its relative abundance is less than 3% in the section, it clearly increased during the glacial MIS 20 and MIS 18 and was absent during MIS 19. Because this species is predominant in Oyashio waters at present (e.g., Kruglikova, 1969), it is likely that the CbCS was in an area where Kuroshio and Oyashio waters mixed.

The Tr value is a radiolarian-based climate index based on the ratio of warm- to cold-water species and was originally proposed by Nigrini (1970). It should serve as a reliable proxy for the Kuroshio

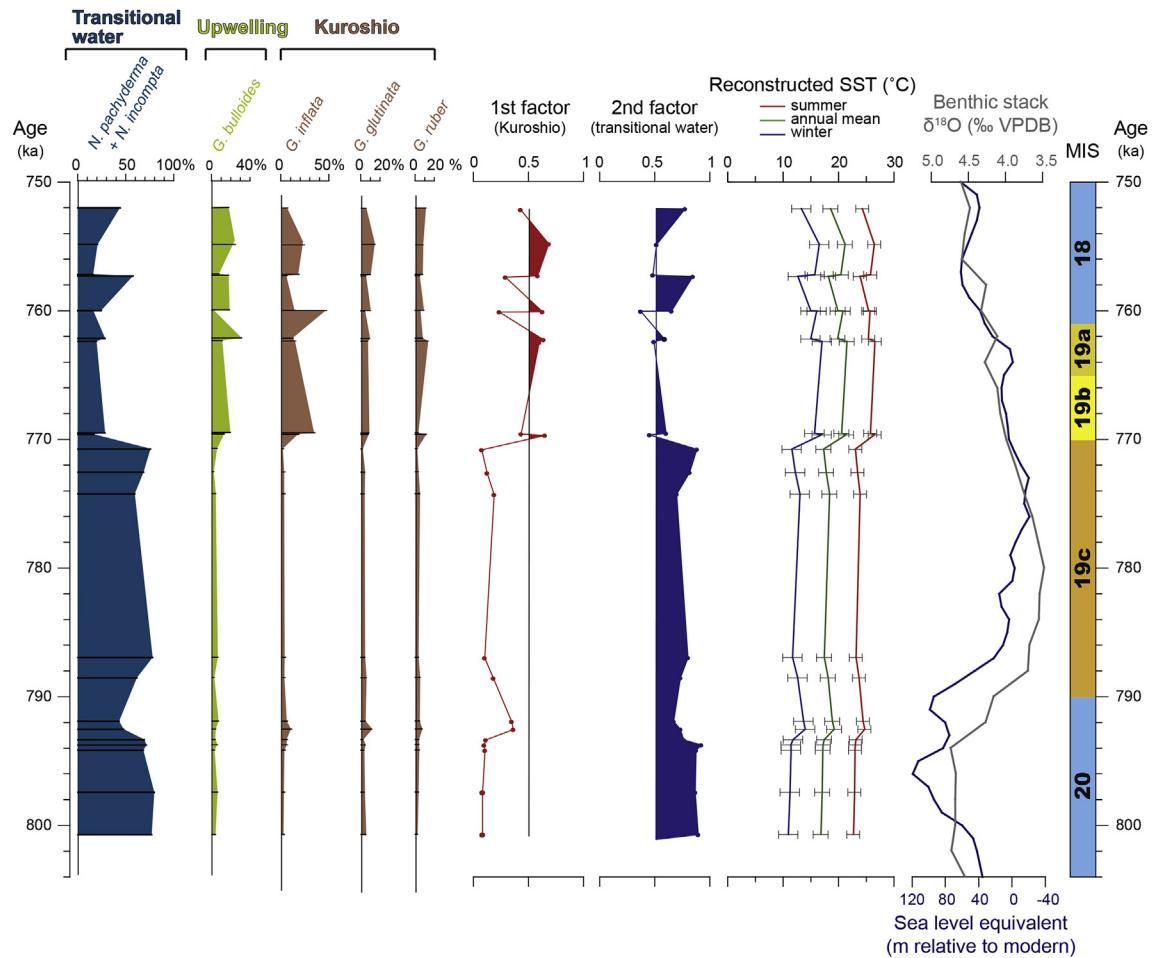


Fig. 8. Relative abundances (%) of selected planktonic foraminifera, varimax factor loadings, and sea surface temperature (SST) reconstructed using PFJ-125 transfer functions (Takemoto and Oda, 1997) at the Chiba composite section (CbCS). The LR04 benthic stack (Lisiecki and Raymo, 2005) and eustatic curve of Elderfield et al. (2012) are shown for comparison.

(high value) and Oyashio (low value) currents in this area. Its value is defined by the following equation.

$$\text{Tr} = \frac{\text{Warm water species}}{\text{Warm water species} + \text{Cold water species}}$$

The radiolarian sea-surface temperature index, the Tr value, fluctuates considerably between 0.2 and 0.8 through the examined interval (Fig. 9), and the several maxima and minima recorded likely reflect oscillations of the Kuroshio Current. This pattern is consistent with the planktonic foraminiferal oxygen isotope record.

Cycladophora davisiana is a known indicator of cold intermediate water (e.g., Itaki and Ikehara, 2004) and tends to increase in relative abundance in MIS 18 and MIS 19b. *Carpocanarium papillosum*, *Cornutella profunda* and *Cyrtopela languncula*, which are also known to be deep dwelling species (e.g., Tanaka and Takahashi, 2008), occur sporadically in the section. The presence of these deep dwellers supports the paleodepth estimation for the CbCS based on the benthic foraminiferal record.

5.3. Foraminiferal geochemistry

5.3.1. Oxygen isotope ($\delta^{18}\text{O}$) stratigraphy

The $\delta^{18}\text{O}_{\text{plank}}$ record of the CbCS is similar to the benthic $\delta^{18}\text{O}$ record, showing pronounced glacial–interglacial cycles from late

MIS 20 to early MIS 18 (Fig. 9). The high cross-correlation coefficients between benthic and planktonic $\delta^{18}\text{O}$ records support this observation (vs. *G. inflata*: $r = 0.858$; vs. *G. bulloides*: $r = 0.779$). In detail, multi-millennial to millennial scale variability is shown in both $\delta^{18}\text{O}_{\text{plank}}$ records in the later part of MIS 19 and during Termination IX. The amplitudes of $\delta^{18}\text{O}_{\text{plank}}$ variations are larger than for the benthic $\delta^{18}\text{O}$ record, suggesting fluctuations in surface–subsurface temperature/salinity. Although salinity variations in the northwestern Pacific Ocean are small (Supplementary fig. 3), the latitudinal temperature gradient in the northwestern Pacific Ocean is significant (Fig. 1a and b). *G. bulloides* and *G. inflata* are most abundant at depths shallower than 50 m and deeper than 100 m, respectively, in the Pacific Ocean off the Japanese archipelago (Arikawa, 1983; Oba and Hattori, 1992; Kuroyanagi and Kawahata, 2004). Because $\delta^{18}\text{O}_{\text{plank}}$ sensitivity to temperature (0.24‰/°C) is higher than for salinity (0.5‰/salinity) (Oba et al., 2006), the $\delta^{18}\text{O}_{\text{plank}}$ records mostly reflect surface (<50 m, *G. bulloides*) and subsurface (>100 m, *G. inflata*) temperature variability. $\delta^{18}\text{O}$ records from *G. bulloides* and *G. inflata* show relatively consistent trends during MIS 19, except during Termination IX and the later part of MIS 19. This suggests that significant surface and subsurface temperature changes occurred during Termination IX perhaps associated with a Younger Dryas-type cooling event.

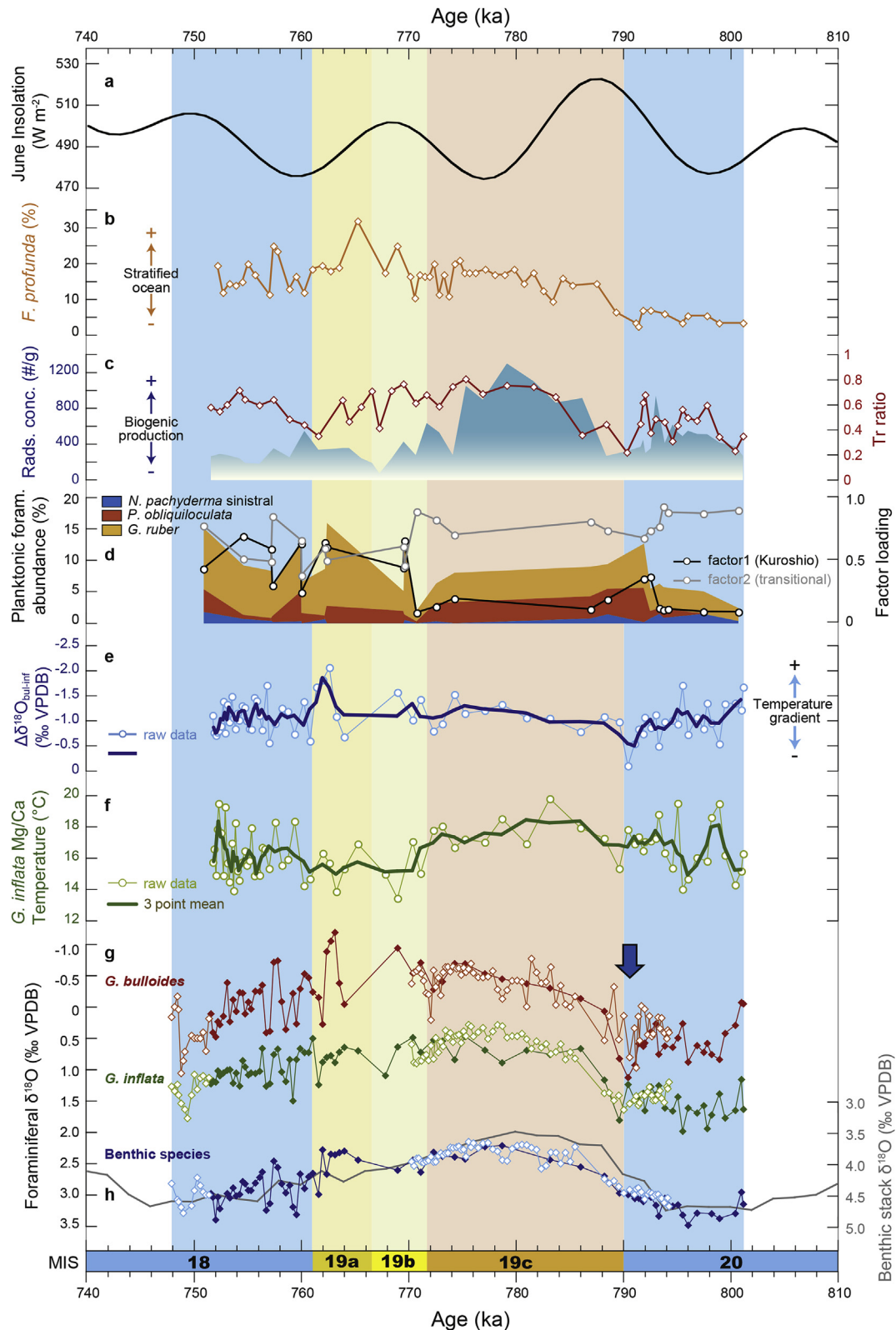


Fig. 9. Paleoclimatic and paleoceanographic records through MIS 20 to MIS 18 from the Chiba composite section (CbCS). (a) 65°N insolation in June. (b) Relative abundance of *F. profunda*. (c) Radiolarian concentrations (~production) and relative abundance of subtropical species. (d) Relative abundance of planktonic foraminifera and results of factor analysis. (e) $\Delta\delta^{18}\text{O}_{\text{bul-inf}}$ (‰ VPDB), corresponding to the temperature gradient between surface and subsurface waters. (f) Mg/Ca paleotemperature for *G. inflata* (T_{inf}). (g) $\delta^{18}\text{O}$ records from the planktonic (*G. bulloides* and *G. inflata*) and benthic foraminifera from the CbCS. The brown/green/blue lines with solid diamonds are from the Yanagawa, Urajiro, and Kokusabata sections (1.0 m spacing), and light orange/light green/light blue lines with open diamonds are from the Yoro River and Yoro-Tabuchi sections (0.2 and 1.0 m spacing) (see Fig. 4). (h) The LR04 benthic stack (Lisiecki and Raymo, 2005). Blue arrow marks the suggested position of the Younger Dryas-type cooling event. (For interpretation of the references to colour in this figure legend, the reader is referred to the Web version of this article.)

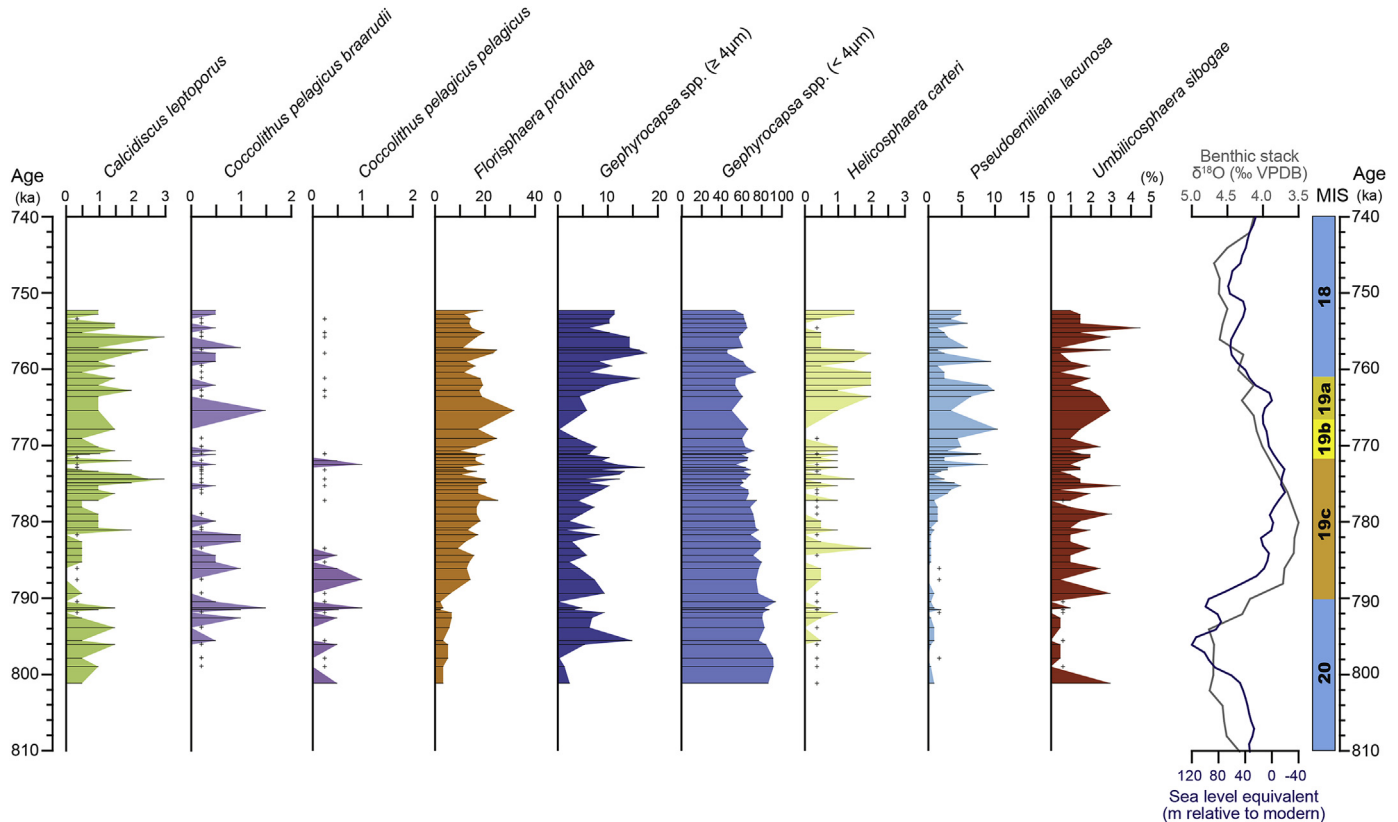


Fig. 10. Stratigraphic distributions and relative abundances of the main calcareous nannofossils from the Chiba composite section (CbCS). The symbol “+” indicates that the species was recorded outside of the count. The LR04 benthic stack (Lisiecki and Raymo, 2005) and the eustatic curve of Elderfield et al. (2012) are shown for comparison.

5.3.2. Mg/Ca

Mg/Ca values were converted to a temperature scale using Anand et al. (2003) and are shown in Fig. 9. The Mg/Ca temperature for *G. inflata* (T_{inf}) is regarded as reflecting the subsurface winter temperature (>100 m) (Oba et al., 2006). The average T_{inf} from late MIS 20 to early MIS 18 is $\sim 17^\circ\text{C}$, showing potential millennial scale variations superimposed on orbital scale variations of the glacial–interglacial cycle. On an orbital scale, the temporal variations show relatively higher winter temperatures from Termination IX to MIS 19c, and lower winter temperatures at MIS 20 and the later part of MIS 19. In addition, T_{inf} reveals millennial scale fluctuations including several spikes of low values during Termination IX.

6. Discussion

6.1. Terrestrial paleoclimate from late MIS 20 to early MIS 18

6.1.1. Japanese archipelago

We have correlated the pollen record from the CbCS to other pollen records in Japan (GS-SB-1, CHOSHI-1, and Osaka Bay in Figs. 1c and 2), as shown by the summary in Fig. 11. The MAT results generated here from earlier published records are based on the same version of Polygon 2.4.4 as used for the CbCS (*Pinus* is also excluded from the analysis). The correlation of these records is initially based on the published age model for each record, and then tuned by the paleomagnetic timescale, $\delta^{18}\text{O}$ records, marker tephra, U–Pb zircon age, etc., as available.

Our palynological data for CbCS are consistent with an adjacent record from a drilled core, GS-SB-1, in the northwestern Kanto Basin (Fig. 2). Although the GS-SB-1 record has low resolution

(Hongo et al., 2011), *Quercus* pollen is abundant across the M–B boundary (Ueki et al., 2009). The *Quercus* zone in GS-SB-1 (264.4–291.1 m in depth) occurs in marine deposits overlain and underlain by terrestrial sediments, therefore likely representing a warm highstand in MIS 19 alternating with sea level lows during MIS 20 and MIS 18. The MAT spectra from MIS 19 in GS-SB-1 suggest paleotemperatures of $9\text{--}10^\circ\text{C}$, consistent with the CbCS.

The CHOSHI-1 core, from the northeast Boso Peninsula (Fig. 2), has yielded a 780 to 400 ka pollen record. The pollen-rich muds of CHOSHI-1 were deposited in stagnant, anaerobic marine environments (Okuda et al., 2006). Although the full interglacial state of MIS 19c is rather ambiguous in CHOSHI-1, the MIS 20–18 obliquity-scale temperature variations are clear.

A 1700-m long sediment core from Higashinada in Osaka Bay (Osaka Bay core) (Fig. 1b) has yielded a detailed MIS 19 pollen record (Kitaba et al., 2009, 2012; 2013, 2017). The upper part of the Osaka Bay core has intermittent marine clay layers (Ma-1 to Ma13) that alternate with freshwater sediments, representing transgressions and regressions due to interglacial–glacial sea level change (Kariya et al., 2010; Kitaba et al., 2011). The authors constructed a 1,000,000 year chronology for this section. MIS 19 is located at a depth of 407–385 m, and contains the M–B boundary at 400.22 m, and the Ma4 marine layer (Hyodo et al., 2006) that was deposited during the sea-level highstand (Biswas et al., 1999) (Fig. 11). Kitaba et al. (2009) documented a marked palynological change and a thermal maximum event at ~ 400 m, at the M–B transition, rather than at the peak of MIS 19. This thermal event is characterized by abundant *Quercus* subgenus *Cyclobalanopsis* (hereafter *Cyclobalanopsis*), an evergreen oak and warm-temperate proxy. However, such a maximum has not been observed in the pollen records of the Kanto basin (CbCS, CHOSHI-1, or GS-SB-1).

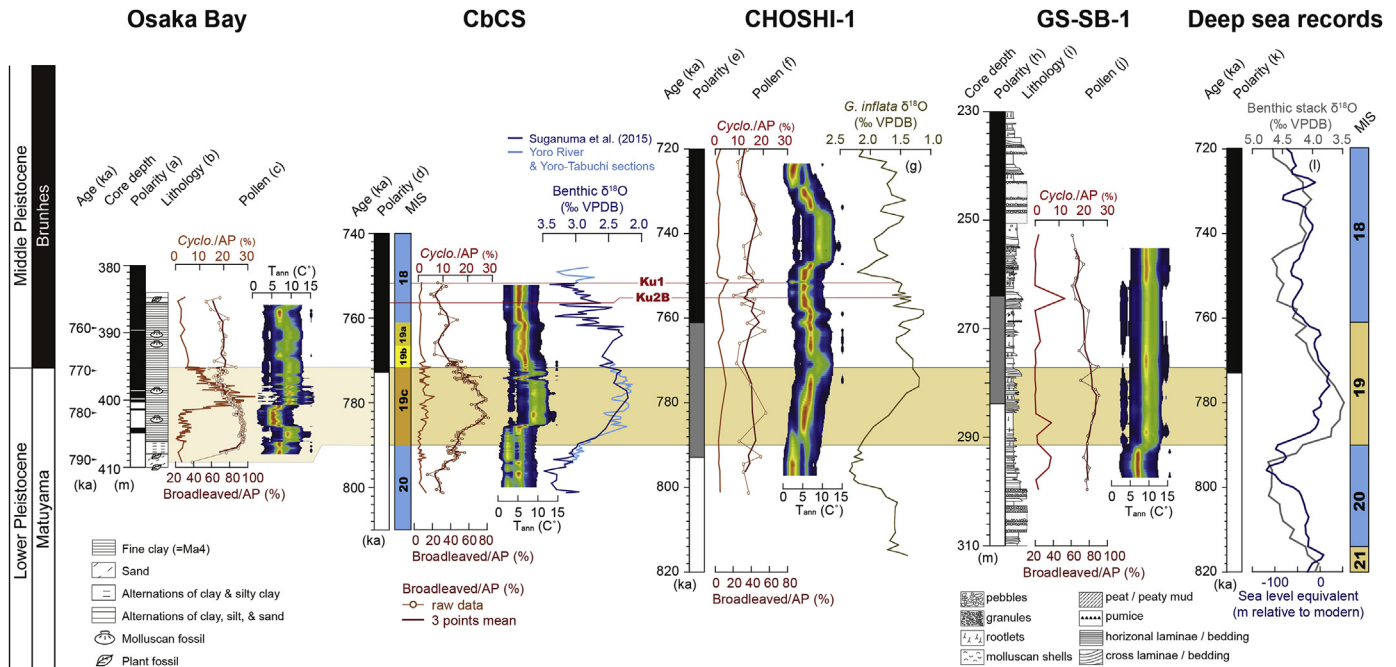


Fig. 11. Comparison of pollen records and marine $\delta^{18}\text{O}$ stratigraphy from late MIS 20 to early MIS 18 between Osaka Bay, Chiba composite section (CbCS), CHOSHI-1 core, and GS-SB-1 core. The warm climate proxy uses the proportion of *Cyclobalanopsis* (evergreen oak), and the ratio of broadleaved trees to total arboreal pollen excluding *Pinus* (broadleaved/AP). Quantified variations of mean annual temperature (T_{ann}), based on the modern analogue technique (MAT) of Nakagawa et al. (2002), are redrawn with the same format; *Pinus* is excluded from the palynoflora, and the latest version of the computing software (Polygon 2.4.4) is used. (a) and (b) Magnetostratigraphy and lithology of the Osaka Bay core (Hyodo et al., 2006). The fine clay interval of the Osaka Bay core corresponds to the Ma4 marine clay, which represents a transgressive phase including the M–B boundary and is assigned to MIS 19 (Hyodo et al., 2006). (c) Pollen record from the Osaka Bay core (Kitaba et al., 2009, 2012; 2013). (d) Magnetostratigraphy of the CbCS is based on Okada et al. (2017). (e) and (g) Magnetostratigraphy and $\delta^{18}\text{O}$ stratigraphy of the CHOSHI-1 core are from Kameo et al. (2006). (f) Pollen record of the CHOSHI-1 core is from Okuda et al. (2006). (h)–(j) Magnetostratigraphy, lithology, and pollen record of the GS-SB-1 core are from Ueki et al. (2009), Naya et al. (2009), and Hongo et al. (2011), respectively. (k) Magnetic polarity time scale (Ogg et al., 2016). (l) Eustatic proxy curve is from Elderfield et al. (2012). The age model of the Osaka Bay core is based on the periodic deposition of transgressive and regressive units, estimated using fluctuations of marine vs freshwater and brackish diatom assemblages within a complex sedimentary setting (Hyodo et al., 2006). The small discrepancy between the Osaka Bay and other records including the M–B boundary horizon may originate with the age model of the Osaka Bay core. Gray shading on the magnetostratigraphy of the GS-SB-1 and CHOSHI-1 cores represents transitional zones (intermediate directions) during the geomagnetic reversal. Chiba composite section: CbCS.

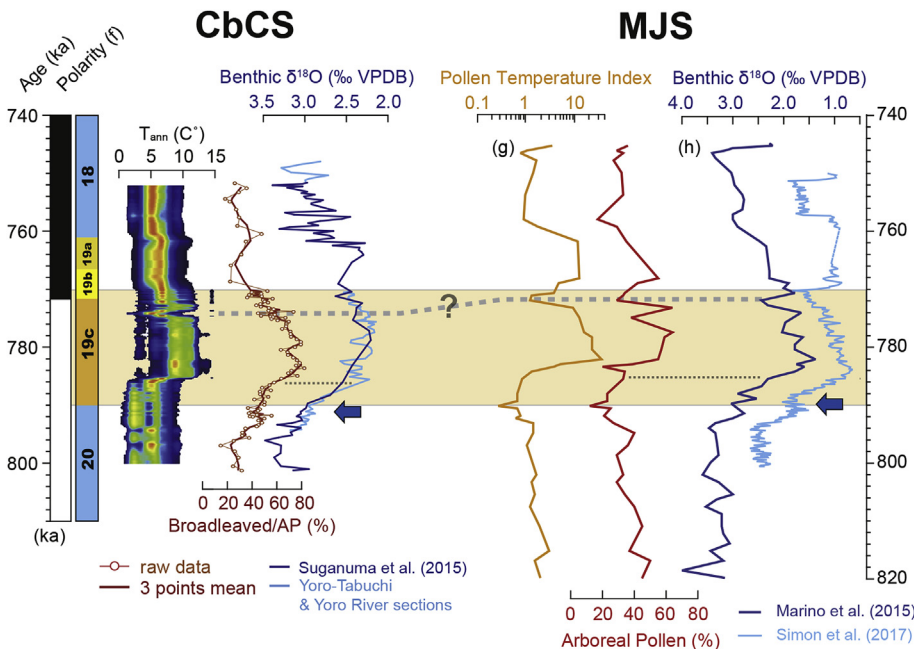


Fig. 12. Comparison of pollen-based indices and marine $\delta^{18}\text{O}$ stratigraphy from late MIS 20 to early MIS 18 between the Chiba composite section (CbCS) and the Montalbano Jonico succession (MJS), southern Italy (Marino et al., 2015; Simon et al., 2017). Thin dashed lines indicate timings of the base of the "MIS 19 plateau" in the CbCS and MJS on the $\delta^{18}\text{O}$ stratigraphy. Horizons of the Younger Dryas-type cooling events in the CbCS and the MJS are shown by blue arrows. (For interpretation of the references to colour in this figure legend, the reader is referred to the Web version of this article.)

Although the timing of the termination and warming and thermal maximum are generally in-phase between records from the Kanto Basin, the apparent delay in the thermal maximum in Osaka Bay requires consideration. Hyodo and Kitaba (2015) interpreted a ~4000 year time lag between the thermal maximum inferred from pollen and the sea level maximum inferred from diatom assemblages (Kitaba et al., 2013). They interpreted a cooling event in the middle of the paleomagnetic intensity low during the M–B transition, and suggested a causal link with the

paleomagnetic reversal.

A possible explanation for this apparent timing relates to the age model of the Osaka Bay core, which was based on sea level records that might have been affected by local as well as eustatic effects. Another source of uncertainty relates to the pollen record of MIS 19 in Japan. In Osaka Bay, *Cyclobalanopsis* in the Ma4 marine clay co-occurs with abundant *Fagus* and *Quercus* subgenus *Lepidobalanus* (Kitaba et al., 2013; Hyodo and Kitaba, 2015). The *Cyclobalanopsis*–*Fagus*–*Lepidobalanus* association is not present in the

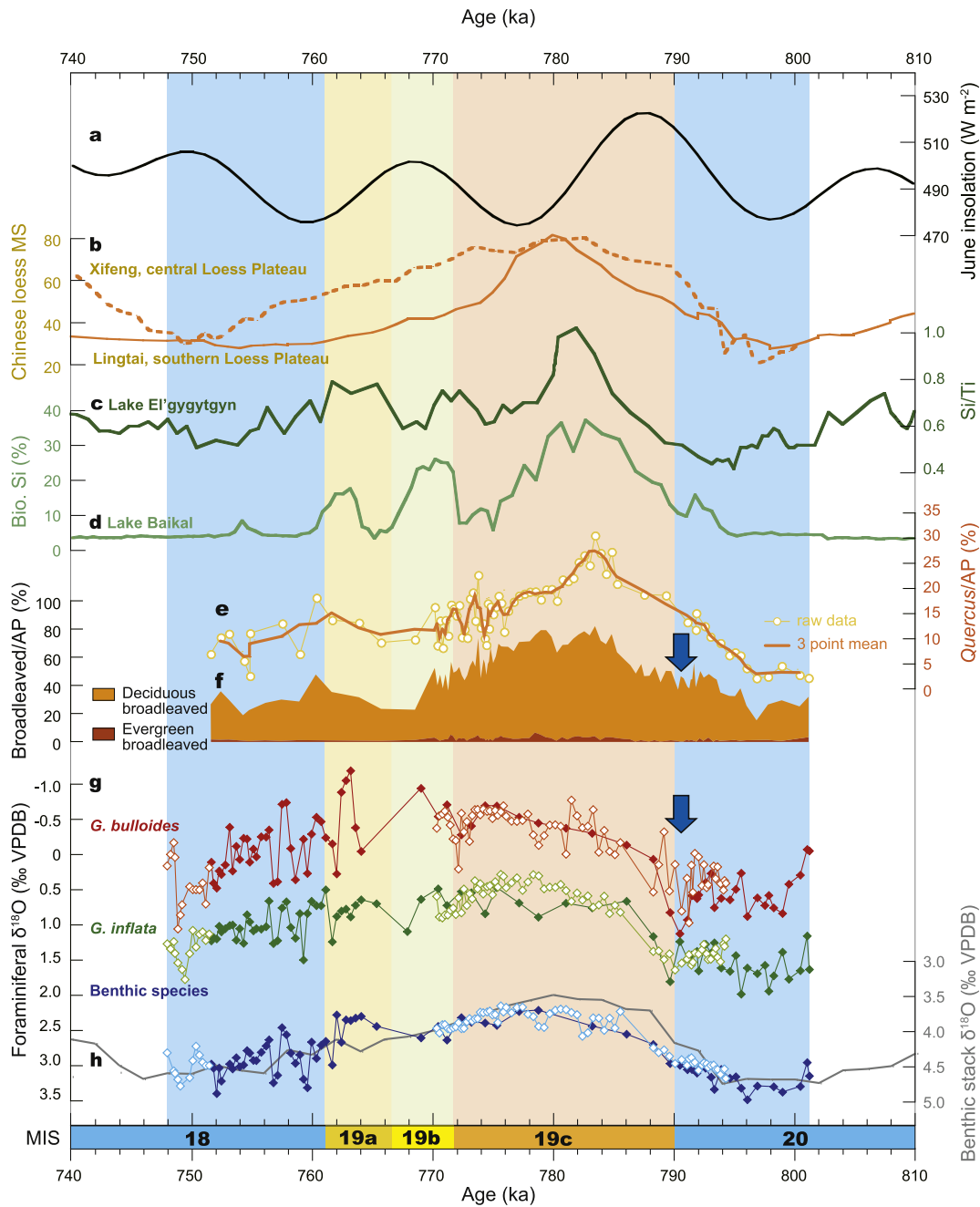


Fig. 13. Paleoclimatic changes during MIS 20 through MIS 18. (a) 65N insolation in June. (b) Magnetic susceptibility (MS) from the Xifeng section of the central Chinese Loess Plateau (Guo et al., 2009), and Lingtai section of the southern Chinese Loess Plateau (Sun et al., 2010). (c) XRF core scanning-derived Si/Ti ratio from Lake El'gygytyn (Wennrich et al., 2014). (d) Biogenic silica contents from Lake Baikal (Prokopenko et al., 2006). (e) and (f) Percentages of *Quercus* subgen. *Lepidobalanus* (%), and evergreen broadleaved trees and deciduous broadleaved trees relative to AP (this study). (g) Planktonic and benthic foraminiferal $\delta^{18}\text{O}$ stratigraphy (this study). The brown/green/blue lines with solid diamonds are from the Yanagawa, Urajiro, and Kokusabata sections (1.0 m spacing), and light orange/light green/light blue lines with open diamonds are from the Yoro River and Yoro-Tabuchi sections (0.2 and 1.0 m spacing). (h) The LR04 benthic stack (Lisiecki and Raymo, 2005). Suggested position of the Younger Dryas-type cooling event is shown by blue arrows. (For interpretation of the references to colour in this figure legend, the reader is referred to the Web version of this article.)

modern vegetation of Japan (Nakanishi et al., 1983) or in surface pollen datasets (Gotanda et al., 2002) because *Cyclobalanopsis* is warm-temperate whereas *Fagus* and *Lepidobalanus* are cool-temperate taxa in Japan (see Fig. 1c). A no-modern-analogue situation would reduce the reliability of the quantitative paleotemperature reconstructions based on MAT. Nevertheless, we acknowledge that our CbCS palynoflora also contains small numbers of taxa such as *Metasequoia* that are no longer present in Japan. This is one reason why we propose here the broadleaved/AP ratio (broadleaved pollen to the total AP excluding *Pinus*) as a substitute temperature proxy. Fig. 11 shows good agreement between the broadleaved/AP trends from Osaka Bay and the CbCS,

and global $\delta^{18}\text{O}$ stratigraphy.

The influence of the geomagnetic field intensity on global climate has been proposed by many workers (Kitaba et al., 2017 and references therein) and it remains a topic of debate. The influence assumes the effects of cloud formation induced by galactic cosmic rays (Svensmark and Friis-Christensen, 1997). Nonetheless, our results from the CbCS are not consistent with those of Osaka Bay. Kitaba et al. (2012) reported a significant cooling coincident with a paleomagnetic intensity low during 785–776 ka in their record. However, the only interpreted cold signal at ~774 ka in the CbCS is less than 2000 years in duration and therefore shorter. Also, the duration of the geomagnetic field-intensity low in the CbCS (Okada

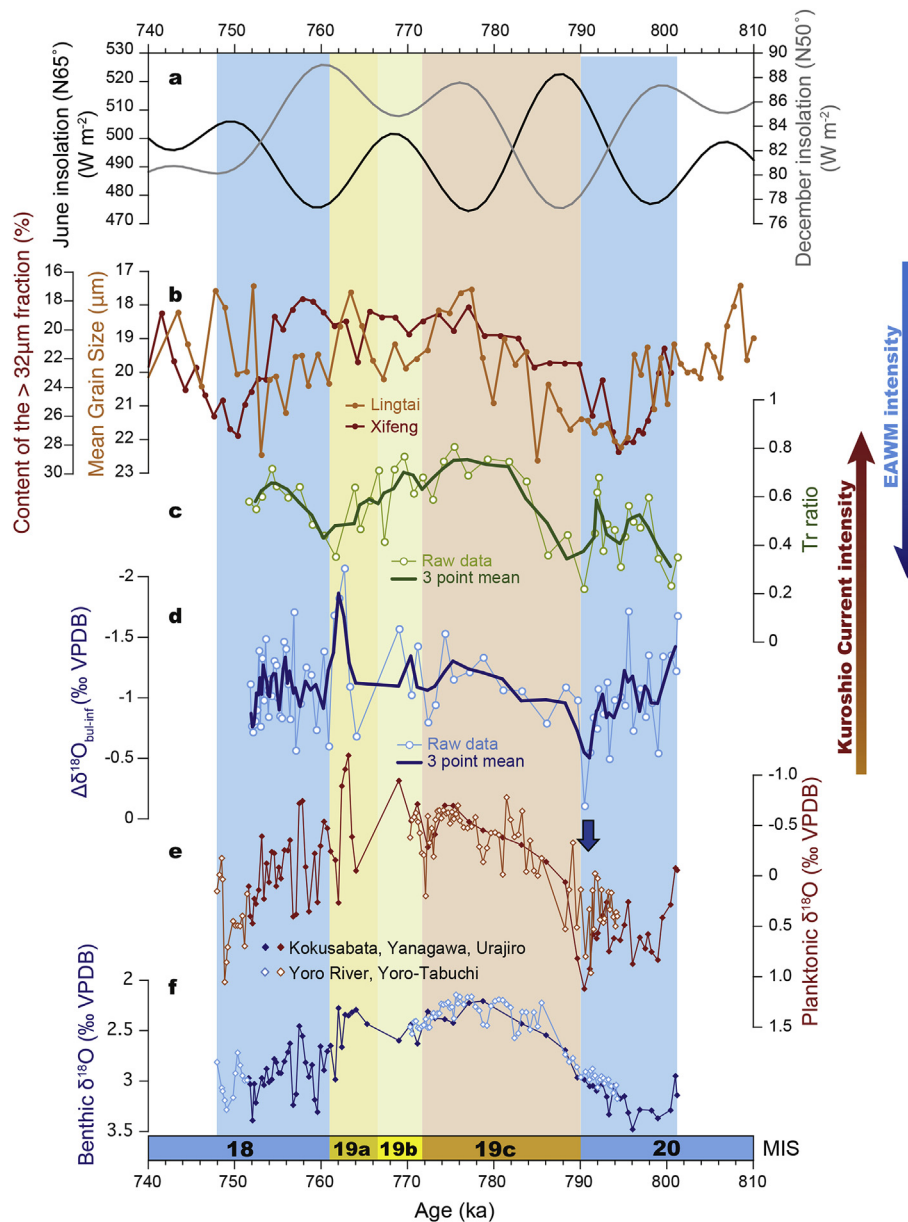


Fig. 14. The Kuroshio Current and East Asian winter monsoon (EAWM) intensity inferred from paleoclimatic and paleoceanographic records of the Chiba composite section (CbCS) and the Chinese loess grain size record. (a) 65N insolation in June and 50N insolation in December. (b) Grain size records from the Xifeng section of the central Chinese Loess Plateau (Guo et al., 2009), and Lingtai section of the southern Chinese Loess Plateau (Sun et al., 2010). (c) Relative subtropical radiolarian abundance (thick red line with open circles from the Yoro River and Yoro-Tabuchi sections). (d) $\delta^{18}\text{O}_{\text{C. bulloides-G. inflata}}$ (bul-inf) (e) and (f) $\Delta\delta^{18}\text{O}$ records of *G. bulloides* and benthic foraminifera from the CbCS. The brown/blue lines with solid diamonds are from the Yanagawa, Urajiro, and Kokusabata sections (1.0 m spacing), and orange and light blue lines with open diamonds are from the Yoro River and Yoro-Tabuchi sections (0.2 and 1.0 m spacing). Suggested position of the Younger Dryas-type cooling event is shown by the blue arrow. (For interpretation of the references to colour in this figure legend, the reader is referred to the Web version of this article.)

et al., 2017) is from 776 to 760 ka based on our new age model. Therefore, a direct coupling between the geomagnetic field intensity and regional/global climate is not apparent from the CbCS record. Further studies on the hypothesized link between the geomagnetic field reversal and terrestrial climate are required.

6.1.2. Northern Hemisphere

A correlation of pollen with benthic $\delta^{18}\text{O}$ records between the CbCS and the MJS in southern Italy (Bertini et al., 2015; Marino et al., 2015; Toti, 2015; Maiorano et al., 2016; Simon et al., 2017) shows that the two records are generally consistent with each other, and the main paleoclimate signals seen in the MJS are observed in the CbCS under higher resolution (Fig. 12). Importantly, a Younger Dryas-type cooling event is recognized during Termination IX in the MJS and in the benthic $\delta^{18}\text{O}$ records of the CbCS, suggesting that these records reflect a global climatic signal. However, the timing of the initiation of full interglacial conditions as inferred from the pollen records is not identical in these two records.

In MJS, the pollen temperature index (PTI) and arboreal pollen percentage (AP%) reflect successive changes in temperature and precipitation, resulting in the alternation between deciduous forest and grassland (Marino et al., 2015) (Fig. 12). Based on this record, Marino et al. (2015) suggested that forest expansion associated with the warm and humid conditions of MIS 19 persisted from 782 to 759.3 ka. Although this onset of warm and humid conditions coincides with MIS 19c (19.3 in their record), the initiation of full interglacial conditions (based on the “MIS 19 plateau”) lags by 1500 years the benthic $\delta^{18}\text{O}$ records of the MJS (thin dashed line in Fig. 12). In contrast, the initiation of full interglacial conditions at the CbCS coincides with changes in the benthic $\delta^{18}\text{O}$ records (based on the “MIS 19 plateau”). In addition, Marino et al. (2015) suggested that the lowering of PTI and AP% values at 771.8 ka and subsequent

increase occurred during MIS 19b and MIS 19a, which may correlate to the brief cooling interval at ~ 774 ka in the CbCS. If this correlation is correct, it implies that MIS 19b is not fully represented in the MJS benthic $\delta^{18}\text{O}$ data.

A correlation between the Japanese archipelago and north-eastern Asian continent is summarized in Fig. 13. The patterns are similar between Japan (CbCS), East Siberia (Lake Baikal and Lake El'gygytyn) and the Chinese Loess Plateau. Prokopenko et al. (2006) documented biogenic silica and diatom maxima at about 786–780 ka, reflecting the highest lacustrine productivity levels during MIS 19c in Lake Baikal. These peaks are followed by two successive highs of biogenic silica (%) representing additional maxima in the later part of MIS 19.

Lake El'gygytyn in the far east of Russia is a ~ 3.6 myr old impact crater lake (Layer, 2000), and provides a unique and continuous sediment archive of the terrestrial Arctic (Wennrich et al., 2016). The Middle and Late Pleistocene interval of this record shows pronounced glacial–interglacial cyclicity (Wennrich et al., 2016), suggesting that the lake and its catchment were strongly susceptible to orbitally-driven climate change. A distinct peak in Si/Ti during MIS 19 is followed by two highs (Fig. 13).

The loess–paleosol sequence of the Chinese Loess Plateau also hosts an important continental archive of past East Asian monsoon variability (e.g., An, 2000). Monsoon variability at orbital to millennial scales, revealed by magnetic susceptibility and particle size, has been dynamically linked to changes in external solar insolation and internal boundary conditions including ice volume and ocean–atmosphere energy exchange (Clemens et al., 2008). The magnetic susceptibility record from the Lingtai section shows a marked peak within MIS 19c (Sun et al., 2010), whereas the Xifeng section shows a broader peak through MIS 19 (Guo et al., 2009) (Fig. 13). This discrepancy may originate from the location of the studied sites and/or the age model between the sections. The

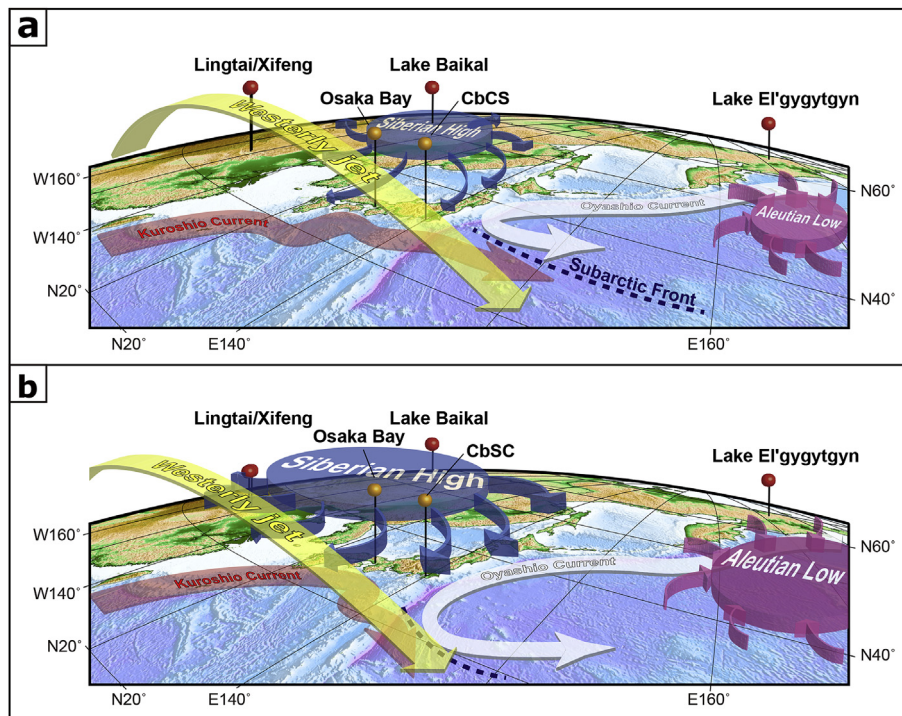
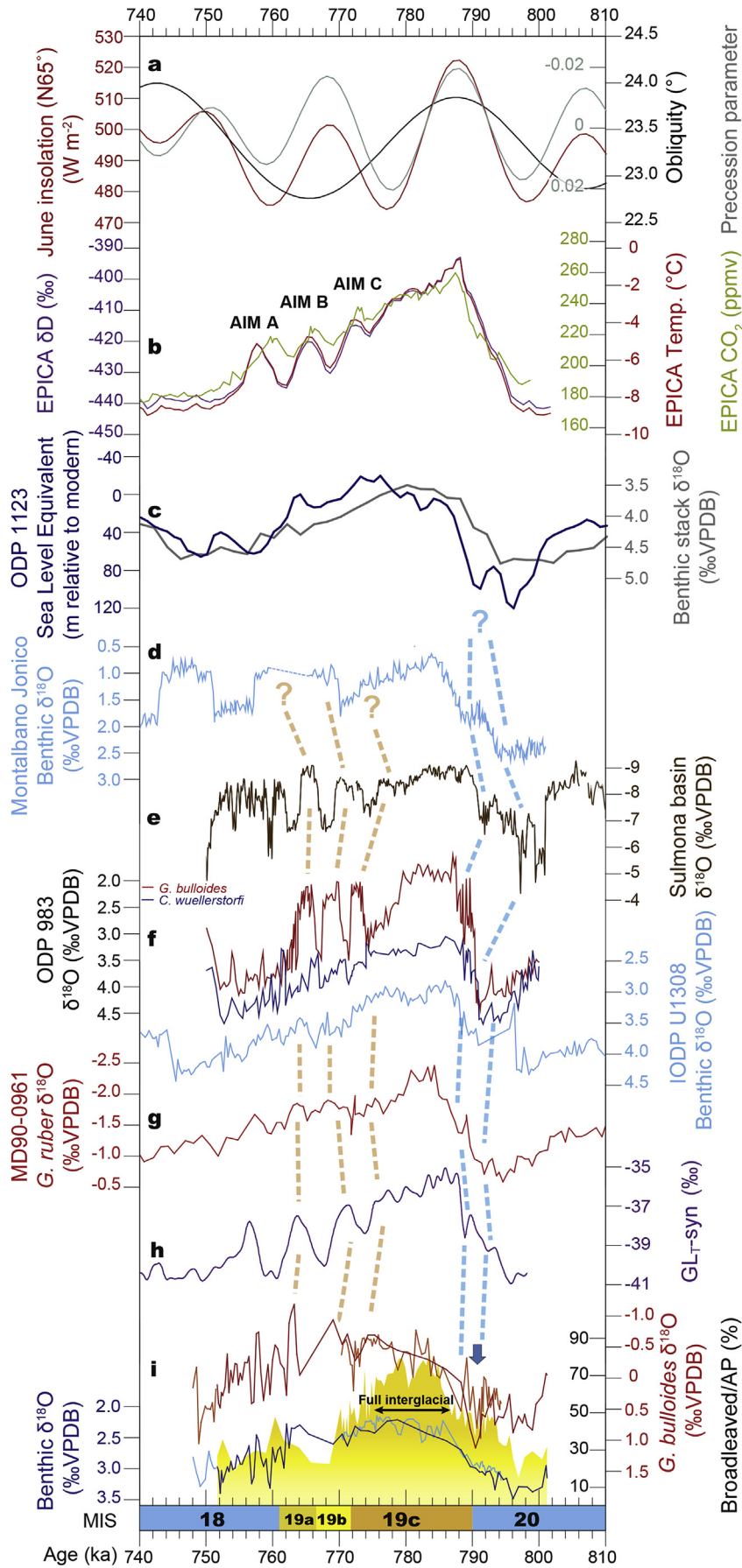


Fig. 15. Schematic representation of the north/south migration of the westerly jet and the Subarctic Front between the subtropical Kuroshio and subarctic Oyashio currents in the northwestern Pacific Ocean. (a) A weaker East Asian winter monsoon (EAWM) led to a northward migration of the Subarctic Front. (b) A stronger EAWM caused the southward migration of the Subarctic Front. Locations of the CbCS, Osaka Bay core, Lake Baikal, Lake El'gygytyn (East Siberia), and Chinese loess paleosol sections (Lingtai and Xifeng) are shown.



chronological framework for loess–paleosol sequences is generally based on paleomagnetic records and is refined using an orbital tuning approach for the last 3.6 Ma (e.g., Sun et al., 2006). However, remagnetization affects the paleomagnetic record of loess–paleosol sequences, and the detection of geomagnetic variations may also be hindered by weak field strength within the sediments, which then requires measurement of multiple sets of subsamples (Liu et al., 2015). The actual position of the M–B boundary in Chinese loess successions has been reviewed in detail by Head and Gibbard (2015a) and Liu et al. (2015), with Head and Gibbard noting the need for more research to resolve issues of equivalency with the marine record.

Records from Lake Baikal, Lake El'gygytgyn, and the Chinese loess–paleosol sequences all show warm climates during MIS 19c, similar to the pollen records of the Pacific margin of east central Japan (Fig. 13). In addition, a Younger Dryas-type cooling event is also recognized during Termination IX in the Lake Baikal record and apparently in the CbCS. These similarities indicate that the climate system in the eastern part of the Eurasian Continent is controlled by a dominant climatic component, presumably involving the Eastern Asian monsoon.

6.2. Paleoceanography

Paleoceanographic records from the CbCS yield surface–subsurface instability in the northwestern Pacific Ocean during Termination IX and the later part of MIS 19 (Fig. 9). During Termination IX, the brief reduction in surface and subsurface temperatures associated with the radiolarian sea-surface temperature index (Tr value) is clearly recognized. The T_{inf} also shows a short plateau during this interval. This paleoceanographic perturbation is thought to be a younger Dryas-type cooling event. For the later part of MIS 19, several minima in the $\delta^{18}O_{plank}$ record of *G. bulloides* suggest high SST events occurring against a global cooling trend toward the next glacial. The marine microfossil records support the existence of these high SST events. For example, the tropical–subtropical planktonic foraminifera *G. ruber* increases in relative abundance during this interval. It is worth noting that the lightest $\delta^{18}O_{plank}$ values for *G. bulloides* and highest relative abundance of *G. ruber* occur after the apparent peak temperatures of MIS 19c.

It is known that variations in the position of the Subarctic Front between the subtropical Kuroshio and subarctic Oyashio currents occurred at orbital (Moore et al., 1980; Thompson and Shackleton, 1980; Chinzei et al., 1987) and millennial time scales, causing large SST changes in the mixing zone between these currents (Oba et al., 2006; Yamamoto et al., 2005). Thus, the warmer SSTs during the later part of MIS 19 most likely correspond to northward shifts of the Subarctic Front. In contrast, the lower T_{inf} and large difference in $\delta^{18}O_{plank}$ between *G. inflata* and *G. bulloides* ($\Delta\delta^{18}O_{bul-inf}$) during this interval suggest a larger vertical density (representing temperature) gradient between surface and subsurface waters and stratification of the ocean (Figs. 9 and 14). This is supported by the near-surface ocean stratification and intensified intermediate

water suggested by the increased abundances of *F. profunda* and *C. davisiana*, respectively. The life span of planktonic foraminifera is thought to be approximately one lunar cycle (Bijma et al., 1990; Hemleben et al., 1989; Spindler et al., 1979; Erez et al., 1991; Jonkers et al., 2015) or several months (Spindler et al., 1979; Jonkers et al., 2010), and *G. bulloides* and *G. inflata* preferentially dwell in the cold seasons around Japan (Kuroyanagi and Kawahata, 2004). Therefore, higher $\Delta\delta^{18}O_{bul-inf}$ values correspond to weaker winter mixing, which is likely to be controlled by the wind strength in winter, namely that of the East Asian winter monsoon (EAWM) (=Siberian High and Aleutian Low). Our observations suggest that the warmer SSTs and slight increase in $\Delta\delta^{18}O_{bul-inf}$ values during the later part of MIS 19 represent a weaker wind-driven mixing and northward migration of the Subarctic Front via a shift in the position of the westerly jet due to the weaker EAWM during this interval (Fig. 15). A weaker EAWM is also confirmed by grain-size variations in loess–paleosol sequences on the Chinese Loess Plateau (Guo et al., 2009; Sun et al., 2010) (Fig. 14), which represents an accepted proxy for the EAWM (e.g., Sun et al., 2006).

The intensity of the EAWM is controlled by the thermal contrast between the Siberian High and Aleutian Low (Fig. 15). In other words, a weak EAWM reflects relatively warmer conditions in Siberia and/or a colder northwestern Pacific Ocean. Hao et al. (2012) suggested that a weak summer insolation minimum at 65N caused a weak Siberian High and resulting weak EAWM winds due to a reduction in ice and snow accumulation in this orbital configuration. However, we here propose that enhanced winter insolation at 50N may also contribute to a weak Siberian High, and consequently a weak EAWM in this orbital configuration and under ice-free conditions (Fig. 14). The relatively small thermal contrast between Siberia and the northwestern Pacific Ocean causes the northern shift of the Subarctic Front and a more stratified near-surface water column (Fig. 15). This hypothesis further suggests that multi-millennial- to millennial-scale fluctuations may be enhanced in this region due to the lower temperature gradient between high and low latitudes.

6.3. Orbital configuration for MIS 19 and the Younger Dryas-type cooling event

The paleoclimatic and paleoceanographic records of the CbCS accord well with glacial–interglacial orbital forcing for the interval from late MIS 20 to early MIS 18. The regional vegetation inferred from the pollen record, and the planktonic foraminiferal records ($\delta^{18}O$ and T_{inf}) all suggest that temperatures in this area were cooler during MIS 19 than today. This is reasonably explained by CO_2 concentrations during MIS 19 (Bereiter et al., 2015) that were lower than Holocene preindustrial CO_2 levels (280 ppm), and conforms to the pattern of stronger interglacials from MIS 11 onwards (Head and Gibbard, 2015a).

In Fig. 16, we compare our late MIS 20 to early MIS 18 records to global datasets. The deuterium isotope record of the EPICA Dome C ice core, $\delta^{18}O$ records from the North Atlantic (IODP Site 1308) and

Fig. 16. Paleoclimatic and paleoceanographic changes through MIS 19. (a) 65N insolation in June and precession parameter and obliquity. (b) Deuterium isotope (Augustin et al., 2004), and temperature change (DTs) (Jouzel et al., 2007) from deuterium content, and CO_2 concentration (Bereiter et al., 2015) records of the European Project for Ice Coring in Antarctica (EPICA) Dome C ice core. (c) LR04 benthic stack (Lisiecki and Raymo, 2005) and sea level proxy (Elderfield et al., 2012). (d) $\delta^{18}O$ record from the Montalbano Jonico succession, Italy (Simon et al., 2017). (e) $\delta^{18}O$ stratigraphy from the Sulmona lake sediments, central Italy (Giaccio et al., 2015). (f) $\delta^{18}O$ records of Ocean Drilling Program (ODP) Site 983 (Channell and Kleiven, 2000) and Integrated Ocean Drilling Program (IODP) Site 1308 (Hodell et al., 2008) from the North Atlantic. (g) $\delta^{18}O$ records from the Indian Ocean (Valet et al., 2014). (h) A synthetic record of Greenland climate variability ($\delta^{18}O$) based on the thermal bipolar seesaw model (Barker et al., 2011). (i) $\delta^{18}O$ stratigraphy of benthic and planktonic foraminifera with the broadleaved pollen percentage (%) from the Chiba composite section. brown/blue lines are from the Yanagawa, Urajiro, and Kokusabata sections (1.0 m spacing), and orange and light blue lines are from the Yoro River and Yoro-Tabuchi sections (0.2 and 1.0 m spacing). A black arrow indicates a length of the full interglacial condition inferred from the pollen record (CbCS-2a). Location of the Younger Dryas-type cooling event is shown by a blue arrow. (For interpretation of the references to colour in this figure legend, the reader is referred to the Web version of this article.)

Indian Ocean (Valet et al., 2014), the LR04 benthic stack (Lisiecki and Raymo, 2005) and the sea level proxy (Elderfield et al., 2012), $\delta^{18}\text{O}$ and CaCO_3 records from the Sulmona lake sediments, central Italy (Giaccio et al., 2015), and a synthetic record of Greenland climate variability based on the thermal bipolar seesaw model (Barker et al., 2011), all show generally similar variations, including their internal structures. A Younger Dryas-type cooling event interrupts Termination IX in the North Atlantic, Indian Ocean, Sulmona lake records, and the synthetic Greenland climatic record, as well as the MJS as already discussed. In the later part of MIS 19, multi-millennial to millennial scale variations are also present. These rapid climatic changes are most likely explained by disruptions/reactivations of the Meridional Overturning Circulation (MOC) (Tzedakis et al., 2012). A similar rapid climatic change in the EPICA Dome C ice core is explained by the bipolar-seesaw mechanism (Stocker and Johnsen, 2003). The generally consistent changes in paleoclimatic and paleoceanographic records, in amplitude and timing, even at the multi-millennial to millennial scale during Termination IX and the later part of MIS 19, suggest teleconnections between the Pacific and Atlantic, and with the Indian Ocean (Fig. 16).

Our pollen data suggest that full MIS 19 interglacial conditions extend from 785.0 to 775.1 ka (9.9 kyr), corresponding to a peak in benthic foraminiferal $\delta^{18}\text{O}$. However, the onset of full interglacial conditions inferred from Mediterranean vegetation records tends to be delayed relative to marine oxygen isotope signals, both in MIS 5a (Shackleton et al., 2003) and MIS 19c (Marino et al., 2015). Since the orbital configurations of MIS 1 and 19 are similar and the vegetation record from the CbCS is generally in phase with global climate change from MIS 20 to 18, this paleoclimatic record appears to be especially well suited for predicting the natural duration of the present interglacial.

In contrast, a discrepancy exists in the Sulmona lake records in terms of the early onset of deglaciation. Although the Sulmona age model is based on high-precision $^{40}\text{Ar}/^{39}\text{Ar}$ chronology, its lacustrine paleoclimatic proxies cannot be directly tuned orbitally. Hence, the putatively old M–B boundary age of 794 ka from the Sulmona lake sediments (Sagnotti et al., 2016; see recalculation in Channell, 2017) requires explanation when compared with recent estimates of 770–774 ka from numerous studies of this boundary elsewhere (e.g., Simon et al., 2018; Channell, 2017; Channell et al., 2016; Head and Gibbard, 2015a; Saganuma et al., 2015; Valet et al., 2014). Although the high precision of $^{40}\text{Ar}/^{39}\text{Ar}$ chronology is acknowledged, its accuracy relies on assumptions that can be questioned (Head and Gibbard, 2015a). Aside from this uncertainty, a recent reanalysis of the paleomagnetic record at Sulmona concludes that this section carries a strong modern overprint and does not preserve a reliable and highly resolvable record of the M–B boundary (Evans and Muxworthy, 2018). It appears therefore that discrepancies in the Sulmona lake records can now be disregarded.

Younger Dryas-type cooling events have rarely been documented in paleoclimate records from the last million years, other than for terminations I and IX (inceptions of MIS 1 and 19). Astronomical configurations (phasing between obliquity and precession) between MIS 1 and 19 are similar and may therefore provide common mechanisms for these events. Based on this similarity, we suggest that the very low eccentricity with the consequent suppression of precessional forcing amplitude, in combination with the obliquity phasing, is a key to triggering the Younger Dryas-type cooling event. It should also be noted that the preceding glacial stages (last glacial maximum and MIS 20–22) for both MIS 1 and 19 were pronounced, and extensive ice sheets may have established conditions favorable for the interruption of deglaciation.

7. Conclusions

The Chiba composite section (CbCS), in the east-central part of the Japanese archipelago facing the northwestern Pacific Ocean, is a well-exposed, continuous and thick marine silty sedimentary succession spanning the Lower–Middle Pleistocene boundary. In this study, we present a new high-resolution foraminiferal $\delta^{18}\text{O}$ stratigraphy for the section, constrained by accurate U–Pb dating and a finely resolved Matuyama–Brunhes polarity reversal. The results show that the section hosts one of the most expanded and complete sedimentary records available for the interval from late MIS 20 to early MIS 18. The M–B boundary has an astronomical age of 772.9 ka and is directly comparable to North Atlantic and Indian Ocean estimates.

New pollen data show that the ratio of broadleaved tree pollen to the total arboreal pollen excluding *Pinus* (broadleaved/AP) significantly expanded during MIS 19c, while boreal coniferous trees decreased during the peak of MIS 19 and then increased again by MIS 18. The vegetation record is consistent with other pollen records from east-central Japan, and generally reproduces paleoclimatic variations seen in the Montalbano Jonico succession (MJS) of southern Italy but at higher resolution. Comparison of the pollen record with paleoclimatic records from eastern Eurasia (Lake Baikal, Lake El'gygytyn, and the Chinese Loess Plateau) suggest that all paleoclimatic perturbations are in-phase, including the Younger Dryas-type cooling event during Termination IX, and millennial-scale climatic instability in the later part of MIS 19. These data suggest that regional-scale vegetational changes from the CbCS reflect glacial–interglacial global climate from late MIS 20 to early MIS 18. The possible influence of Earth's magnetic field intensity on regional/global climate, as recently suggested from the pollen record of Osaka Bay in western Japan, is not supported by our record.

Mg/Ca paleotemperatures for *G. inflata* (T_{inf}) and radiolarian concentrations, both from the CbCS, suggest that ocean temperatures and biogenic production in the northwestern Pacific Ocean were modulated by glacial–interglacial orbital forcing from late MIS 20 to early MIS 18. In addition, marine microfossil assemblages and $\delta^{18}\text{O}$ planktonic trends reveal clear multi-millennial to millennial scale variations during Termination IX and the later part of MIS 19. Data from our paleoceanographic proxies indicate that fluctuations of the Subarctic Front in the northwestern Pacific occurred during glacial to interglacial, and interglacial to glacial, transitions.

The northward migration of the Kuroshio Current at ~770 ka following the MIS 19 maximum, influenced by the North Pacific–Siberian pressure contrasts, is thought to be caused by a weakening of the EAWM (East Asian winter monsoon). Although the less-severe summer insolation minima at 65N have been proposed as the cause of the weak Siberian High (Hao et al., 2012), we also suggest that enhanced winter insolation at 50N led to the weak Siberian High, and a weak EAWM in this orbital configuration. Due to the smaller temperature gradient between the high and low latitudes of East Asia, multi-millennial- to millennial-scale climatic and paleoceanographic fluctuations may be enhanced in the later part of MIS 19 in this setting.

Regional vegetation and geochemical records (oceanic paleotemperature proxies) suggest that the temperature in this area was lower during MIS 19 than today, which is reasonably explained by the lowered atmospheric CO_2 concentrations during MIS 19 (Bereiter et al., 2015). The duration of full interglacial conditions during MIS 19 is estimated to be 9.9 kyr (785.0–775.1 ka) which has relevance in predicting the natural duration of the present interglacial. Paleoclimatic records from other sites in the Northern Hemisphere, including the CbCS, show persistent multi-millennial to millennial scale variations, especially during Termination IX

and the later part of MIS 19. These synchronous changes suggest Pacific, Atlantic, and Indian teleconnections. We propose that the reduced amplitude of the 400-ky eccentricity cycle and precessional forcing combined with the obliquity phasing, along with extensive preceding glaciations, may have triggered the Younger Dryas-type cooling events in terminations I and IX (MIS 1 and 19).

Our records of the CbCS demonstrate the importance of millennial-scale resolution in understanding the Earth's climate system, especially during MIS 19. The M–B boundary is the primary chronological marker for the Lower–Middle Pleistocene Subseries boundary (Head et al., 2008), which is in the process of being defined by a Global Boundary Stratotype Section and Point (GSSP; Head and Gibbard, 2015b). Our detailed analyses show that the CbCS would serve as a uniquely suitable location for the Middle Pleistocene GSSP.

Acknowledgements

This study was supported by a JSPS Kakenhi Grant (16H04068; 15K13581; 17H06320; 17H06321), the Center for the Promotion of Integrated Sciences (CPIS) of Sokenai, NIPR through an Advanced Project (KP-7 and KP301), and the grants “Rebuilding of Micropaleontological Reference Center collections” and “Chemical stratigraphy and dating” at the National Museum of Nature and Science. We thank Osamu Kazaoka and Atsushi Kagawa for providing information on the lateral distributions of key tephra beds. It is a pleasure to thank all those who have co-operated with us on this project, from the Tabuchi district, Ichihara City, Chiba prefecture, and Ministry of Education, for their kind support. Constructive comments received during the review process are greatly appreciated.

Appendix A. Supplementary data

Supplementary data related to this article can be found at <https://doi.org/10.1016/j.quascirev.2018.04.022>.

References

- Aida, N., 1997. Paleomagnetic stratigraphy of the type section (proposed site) for the lower/middle Pleistocene boundary Kokumoto Formation. In: Kawamura, M., Oka, T., Kondo, T. (Eds.), *Commemorative Volume for Professor Makoto Kato*, pp. 275–282 (in Japanese with English abstract).
- An, Z.S., 2000. The history and variability of the East Asian paleomonsoon climate. *Quat. Sci. Rev.* 19, 171–187. [https://doi.org/10.1016/S0277-3791\(99\)00060-8](https://doi.org/10.1016/S0277-3791(99)00060-8).
- Anand, P., Elderfield, H., Conte, M.H., 2003. Calibration of Mg/Ca thermometry in planktonic foraminifera from a sediment trap time series. *Paleoceanography* 18 (2), 1050. <https://doi.org/10.1029/2002PA000846>.
- Arikawa, R., 1983. Distribution and taxonomy of *Globigerina pachyderma* (Ehrenberg) off the Sanriku coast, northeast Honshu, Japan. *Sci. Rep. Tohoku Univ., 2nd ser. (Geol.)*, 53, pp. 103–157.
- Augustin, L., Barbante, C., Barnes, P.R.F., Barnola, J.M., Bigler, M., Castellano, E., Cattani, O., Chappellaz, J., Dahljensen, D., Delmonte, B., Dreyfus, G., Durand, G., Falourd, S., Fischer, H., Flückiger, J., Hansson, M.E., Huybrechts, P., Jugie, R., Johnsen, S.J., Jouzel, J., Kaufmann, P., Kipfstuhl, J., Lambert, F., Lipenkov, V.Y., Littot, G.V.C., Longinelli, A., Lorrain, R., Maggi, V., Masson-Delmotte, V., Miller, H., Mulvaney, R., Oerlemans, J., Oerter, H., Orlandini, G., Parrenin, F., Peel, D.A., Petit, J.R., Raynaud, D., Ritz, C., Ruth, U., Schwander, J., Siegenthaler, U., Souchez, R., Stauffer, B., Steffensen, J.P., Stenni, B., Stocker, T.F., Tabacco, I.E., Udisti, R., van de Wal, R.S.W., van den Broeke, M., Weiss, J., Wilhelms, F., Winther, J.G., Wolff, E.W., Zucchielli, M., 2004. Eight glacial cycles from an Antarctic ice core. *Nature* 429, 623–628. <https://doi.org/10.1038/nature02599>.
- Barker, S., Knorr, G., Edwards, R.L., Parrenin, F., Putnam, A.E., Skinner, L.C., Wolff, E., Ziegler, M., 2011. 800,000 years of abrupt climate variability. *Science* 334, 347–351. <https://doi.org/10.1126/science.1203580>.
- Bereiter, B., Eggleston, S., Schmitt, J., Nehrbass-Ahles, C., Stocker, T.F., Fischer, H., Kipfstuhl, S., Chappellaz, J., 2015. Revision of the EPICA Dome C CO₂ record from 800 to 600 kyr before present. *Geophys. Res. Lett.* 42, 542–549. <https://doi.org/10.1002/2014GL061957>.
- Berger, B., Crucifix, M., Hodell, D.A., Mangili, C., McManus, J.F., Otto-Bliesner, B., Pol, K., Raynaud, D., Skinner, L.C., Tzedakis, P.C., Wolff, E.W., Yin, Q.Z., Abe-Ouchi, A., Barbante, C., Brovkin, V., Cacho, I., Capron, E., Ferretti, P., Ganopolski, A., Grimalt, J.O., Hönisch, B., Kawamura, K.A., Landais, A., Margari, V., Martrat, B., Masson-Delmotte, V., Mokeddem, Z., Parrenin, F., Prokopenko, A.A., Rashid, H., Schulz, M., Vazquez Riveiros, N., 2016. Interglacials of the last 800,000 years. *Rev. Geophys.* 54, 162–219. <https://doi.org/10.1002/2015RG000482>.
- Berger, W.H., Yasuda, M.K., Bickert, T., Wefer, G., Takayama, T., 1994. Quaternary time-scale for the Ontong Java Plateau: Milankovitch template for Ocean Drilling Program Site 806. *Geology* 22, 463–467. [https://doi.org/10.1130/0091-7613\(1994\)022<0463:QTSFTO>2.3.CO;2](https://doi.org/10.1130/0091-7613(1994)022<0463:QTSFTO>2.3.CO;2).
- Bertini, A., Toti, F., Marino, M., Ciaranfi, N., 2015. Vegetation and climate across the early-middle Pleistocene transition at Montalbano Jonico, southern Italy. *Quat. Int.* 383, 74–88. <https://doi.org/10.1016/j.quaint.2015.01.003>.
- Bijma, J., Erez, J., Hemleben, C., 1990. Lunar and semi-lunar reproductive cycles in some spinose planktonic foraminifers. *J. Foramin. Res.* 20, 117–120. <https://doi.org/10.2113/gsjfr.20.2.117>.
- Biswas, D.K., Hyodo, M., Taniguchi, Y., Kaneko, M., Katoh, S., Sato, H., Kinugasa, Y., Mizuno, K., 1999. Magnetostratigraphy of Plio-Pleistocene sediments in a 1700-m core from Osaka Bay, southwestern Japan and short geomagnetic events in the middle Matuyama and early Brunhes chrons. *Palaeogeogr. Palaeoclimatol. Palaeoecol.* 148, 233–248. [https://doi.org/10.1016/S0031-0182\(98\)00185-0](https://doi.org/10.1016/S0031-0182(98)00185-0).
- Blow, W.H., 1969. Late middle Eocene to recent planktonic foraminiferal biostratigraphy. In: Brönnimann, P., Renz, H.H. (Eds.), *Proceedings of the First International Conference on Planktonic Microfossils*, Geneva, 1967, 1. E.J. Brill, Leiden, pp. 199–422.
- Boyle, E.A., Keigwin, L., 1987. North Atlantic thermohaline circulation during the past 20000 years linked to high-latitude surface temperature. *Nature* 330, 35–40. <https://doi.org/10.1038/330035a0>.
- Brown, E., Colling, A., Park, D., Phillips, J., Rothery, D., Wright, J., 2001. Chapter 3 – Ocean Currents, Ocean Circulation (Second Edition). Butterworth-Heinemann, Oxford, pp. 37–78.
- Channell, J.E.T., 2017. Complexity in Matuyama–Brunhes polarity transitions from North Atlantic IODP/ODP deep-sea sites. *Earth Planet. Sci. Lett.* 467, 43–56. <https://doi.org/10.1016/j.epsl.2017.03.019>.
- Channell, J.E.T., Hodell, D.A., Curtis, J.H., 2016. Relative paleointensity (RPI) and oxygen isotope stratigraphy at IODP Site U1308: Sub Atlantic RPI stack for 1.2–2.2 Ma (NARPI-2200) and age of the Olduvai Subchron. *Quat. Sci. Rev.* 131, 1–19. <https://doi.org/10.1016/j.quascirev.2015.10.011>.
- Channell, J.E.T., Kleiven, H.F., 2000. Geomagnetic paleointensities and astrochronological ages for the Matuyama–Brunhes boundary and the boundaries of the Jaramillo Subchron: paleomagnetic and oxygen isotope records from ODP Site 983. *Philos. Trans. R. Soc. Lond. Ser. A – Math. Phys. Eng. Sci.* 358, 1027–1047. <https://doi.org/10.1098/rsta.2000.0572>.
- Cherepanova, M.V., Pushkar, V.S., Razjigaeva, N., Kumai, H., Koizumi, I., 2002. Diatom biostratigraphy of the Kazusa Group, Boso Peninsula, Honshu, Japan. *Quat. Res. (Daiyonki Kenkyu)* 41, 1–10.
- Chiba Prefecture, 2004 (. Report of Seismic Geological Survey in Chiba Prefecture. Chiba Prefecture, Japan in Japanese).
- Chinzei, K., Fujioka, K., Kitazato, H., Koizumi, I., Oba, T., Oda, M., Okada, H., Sakai, T., Tanimura, Y., 1987. Postglacial environmental change of the Pacific Ocean off the coasts of central Japan. *Mar. Micropaleontology* 11, 273–291. [https://doi.org/10.1016/0377-8398\(87\)90002-8](https://doi.org/10.1016/0377-8398(87)90002-8).
- Clark, P.U., Archer, D., Pollard, D., Blum, J.D., Rial, J.A., Brovkin, V., Mix, A.C., Piasis, N.G., Roy, M., 2006. The middle Pleistocene transition: characteristics, mechanisms, and implications for long-term changes in atmospheric pCO₂. *Quat. Sci. Rev.* 25, 3150–3184. <https://doi.org/10.1016/j.quascirev.2006.07.008>.
- Clemens, S.C., Prell, W.L., Sun, Y., Liu, Z., Chen, G., 2008. Southern Hemisphere forcing of Pliocene δ¹⁸O and the evolution of Indo-Asian monsoons. *Paleoceanography* 23. <https://doi.org/10.1029/2008PA001638>.
- El-Masry, M.M.I., 2002. Sedimentation and Physical Property Variability of Hemipelagic Mudstone in Response to the Pleistocene Glacial and Interglacial Cycles. PhD dissertation. University of Tokyo, Japan.
- Elderfield, H., Ferretti, P., Greaves, M., Crowhurst, S., McCave, I.N., Hodell, D., Piotrowski, A.M., 2012. Evolution of ocean temperature and ice volume through the mid-Pleistocene climate transition. *Science* 337, 704–709. <https://doi.org/10.1126/science.1221294>.
- Erez, J., Almogi-Labin, A., Avraham, S., 1991. On the life history of planktonic foraminifera: lunar reproduction cycle in *Globigerinoides sacculifer* (Brady). *Paleoceanography* 6, 295–306. <https://doi.org/10.1029/90pa02731>.
- Evans, M.E., Muxworthy, A.R., 2018. A re-appraisal of the proposed rapid Matuyama–Brunhes geomagnetic reversal in the Sulmona Basin, Italy. *Geophys. J. Int.* <https://doi.org/10.1093/gji/ggy111>.
- Gallagher, S.J., Kitamura, A., Iryu, Y., Itaki, T., Koizumi, I., Hoiles, P.W., 2015. The Pliocene to recent history of the Kuroshio and Tsushima Currents: a multiproxy approach. *Prog. Earth Planet. Sci.* 2, 17. <https://doi.org/10.1186/s40645-015-0045-6>.
- Ganopolski, A., Winkelmann, R., Schellnhuber, H.J., 2016. Critical insolation–CO₂ relation for diagnosing past and future glacial inception. *Nature* 529, 200–203. <https://doi.org/10.1038/nature16494>.
- Giaccio, B., Regattieri, E., Zanchetta, G., Nomade, S., Renne, P.R., Sprain, C.J., Drysdale, R.N., Tzedakis, P.C., Messina, P., Scardia, G., Sposato, A., Bassinot, F., 2015. Duration and dynamics of the best orbital analogue to the present interglacial. *Geology* 43, 603–606. <https://doi.org/10.1130/G36677.1>.
- Gotanda, K., Nakagawa, T., Tarasov, P., Kitagawa, J., Inoue, Y., Yasuda, Y., 2002. Biome classification from Japanese pollen data: application to modern-day and Late Quaternary samples. *Quat. Sci. Rev.* 21, 647–657.

- 3791(01)00046-4.
- Guo, Z.T., Berger, A., Yin, Q.Z., Qin, L., 2009. Strong asymmetry of hemispheric climates during MIS-13 inferred from correlating China loess and Antarctica ice records. *Clim. Past* 5, 21–31. <https://doi.org/10.5194/cp-5-21-2009>.
- Hao, Q., Wang, L., Oldfield, F., Peng, S., Qin, L., Song, Y., Xu, B., Qiao, Y., Bloemendal, J., Guo, Z., 2012. Delayed build-up of Arctic ice sheets during 400,000-year minima in insolation variability. *Nature* 490, 393–396. <https://doi.org/10.1038/nature11493>.
- Head, M.J., Gibbard, P.L., 2005. Early–Middle Pleistocene transitions: an overview and recommendation for the defining boundary. In: Head, M.J., Gibbard, P.L. (Eds.), *Early–Middle Pleistocene Transitions: The Land–ocean Evidence*. Geological Society, London, Special Publication, vol. 247, pp. 1–18.
- Head, M.J., Gibbard, P.L., 2015a. Early–Middle Pleistocene transitions: linking terrestrial and marine realms. *Quat. Int.* 389, 7–46. <https://doi.org/10.1016/j.quaint.2015.09.042>.
- Head, M.J., Gibbard, P.L., 2015b. Formal subdivision of the Quaternary System/Period: past, present, and future. *Quat. Int.* 383, 4–35. <https://doi.org/10.1016/j.quaint.2015.06.039>.
- Head, M.J., Pillans, B., Farquhar, S.A., 2008. The Early–Middle Pleistocene transition: characterization and proposed guide for the defining boundary. *Episodes* 31, 255–259.
- Hemleben, C., Spindler, M., Anderson, O.R., 1989. *Modern Planktonic Foraminifera*. Springer Verlag, Berlin, 363 pp.
- Heusser, L.E., 1990. Northeast Asian pollen records for the last 150,000 years from deep-sea cores V28–304 and RC14–99 taken off the Pacific coast of Japan. *Rev. Palaeobot. Palynol.* 65, 1–8. [https://doi.org/10.1016/0034-6667\(90\)90050-S](https://doi.org/10.1016/0034-6667(90)90050-S).
- Hodell, D.A., Channell, J.E.T., Curtis, J.H., Romero, O.E., Röhl, U., 2008. Onset of “Hudson Strait” Heinrich events in the eastern North Atlantic at the end of the middle Pleistocene transition (~640 ka)? *Paleoceanography* 23, PA4218. <https://doi.org/10.1029/2008PA001591>.
- Hodell, D.A., Lourens, L., Stow, D.A.V., Hernández-Molina, J., Alvarez Zarikian, C.A., Shackleton Site Project Members, 2013. The “Shackleton site” (IODP Site U1385) on the Iberian Margin. *Sci. Drill.* 16, 13–19. <https://doi.org/10.5194/sd-16-13-2013>.
- Hongo, M., Naya, T., Yamaguchi, M., Mizuno, K., 2011. Pollen assemblages of GS-SB-1 drilling core at Shobu Town, Saitama Prefecture, central Kanto plain, Japan. *Bull. Geol. Surv. Jpn.* 62, 281–318 (in Japanese with English abstract).
- Hubbard, S.M., MacEachern, J.A., Bann, K.L., 2012. Slopes. In: Knaust, D., Bromley, R.G. (Eds.), *Trace Fossils as Indicators of Sedimentary Environments*. Developments in Sedimentology, vol. 64, pp. 607–642.
- Hyodo, M., Kitaba, I., 2015. Timing of the Matuyama-Brunhes geomagnetic reversal: decoupled thermal maximum and sea-level highstand during Marine Isotope Stage 19. *Quat. Int.* 383, 136–144. <https://doi.org/10.1016/j.quaint.2015.01.052>.
- Hyodo, M., Biswas, D.K., Noda, T., Tomioka, N., Mishima, T., Itota, C., Sato, H., 2006. Millennial- to submillennial-scale features of the Matuyama-Brunhes geomagnetic polarity transition from Osaka Bay, southwestern Japan. *J. Geophys. Res.* 111, B02103. <https://doi.org/10.1029/2004jb003584>.
- Hyodo, M., Katoh, S., Kitamura, A., Takasaki, K., Matsushita, H., Kitaba, I., Tanaka, I., Nara, M., Matsuzaki, T., Dettman, D.L., Okada, M., 2016. High resolution stratigraphy across the early–middle Pleistocene boundary from a core of the Kokumoto Formation at Tabuchi, Chiba prefecture, Japan. *Quat. Int.* 397, 16–26. <https://doi.org/10.1016/j.quaint.2015.03.031>.
- Igarashi, A., 1994. Paleoenvironmental changes during the deposition of the middle Pleistocene Kazusa Group, central Japan: estimation based on the principal components analysis of planktonic foraminifera. *Jour. Geol. Soc. Jpn.* 100, 348–359 (in Japanese with English abstract).
- Igarashi, A., 1996. Biostratigraphy of the Chiba section of the Boso Peninsula toward establishing the Lower–Middle Pleistocene boundary stratotype based on planktonic foraminiferal analyses. *Proc. Res. stratotype Lower–Middle Pleistocene Bound.* 36–45.
- Igarashi, A., Kamemaru, A., 2011. Biostratigraphy of the Chiba section of the Boso Peninsula toward establishing the lower-middle Pleistocene boundary stratotype based on planktonic and benthic foraminiferal analyses. In: *International Symposium on Type Section for Lower–Middle Pleistocene Boundary*, Ichihara city, Japan. *Proc. Vol.* 51–55.
- Imbrie, J., Kipp, N.G., 1971. A new micropaleontological method for quantitative paleoclimatology: application to a late Pleistocene Caribbean core. In: Turekian, K.K. (Ed.), *The Late Cenozoic Glacial Ages*. Yale University Press, New Haven, pp. 71–181.
- Itaki, T., Ikehara, K., 2004. Middle to late Holocene changes of the Okhotsk Sea intermediate water and their relation to atmospheric circulation. *Geophys. Res. Lett.* 31, L24309. <https://doi.org/10.1029/2004GL021384>.
- Itaki, T., Uchida, M., Kim, S., Shin, H.-S., Tada, R., Khim, B.-K., 2009. Late Pleistocene stratigraphy and paleoenvironmental implications in northern Bering Sea slope sediments: evidence from the radiolarian species *Cycladophora davidiana*. *Jour. Quat. Sci.* 24, 856–865. <https://doi.org/10.1002/jqs.1356>.
- Ithara, M., Kamei, T., Mitsunashi, T., Suzuki, K., Kuwano, Y., 1973. The basis of the Plio-Pleistocene boundary in Japan. *J. Geosciences, Osaka City Univ.* 16 (Art. 3), 25–49.
- Ito, M., 1992. High-frequency depositional sequences of the upper part of the Kazusa Group, a middle Pleistocene forearc basin fill in Boso Peninsula, Japan. *Sediment. Geol.* 76, 155–175. [https://doi.org/10.1016/0037-0738\(92\)90081-2](https://doi.org/10.1016/0037-0738(92)90081-2).
- Ito, M., 1998. Submarine fan sequences of the lower Kazusa Group, a Plio-Pleistocene forearc basin fill in the Boso Peninsula, Japan. *Sediment. Geol.* 122, 69–93. [https://doi.org/10.1016/S0037-0738\(98\)00099-2](https://doi.org/10.1016/S0037-0738(98)00099-2).
- Ito, M., Kameo, K., Satoguchi, Y., Masuda, F., Hiroki, Y., Takano, O., Nakajima, T., Suzuki, N., 2016. Neogene–Quaternary sedimentary successions. In: Moreno, T., Wallis, S., Kojima, T., Gibbons, W. (Eds.), *The Geology of Japan*. Geological Society, London, pp. 309–337.
- Ito, M., Katsura, Y., 1992. Inferred glacio-eustatic control for high-frequency depositional sequences of the Plio-Pleistocene Kazusa Group, a forearc basin fill in Boso Peninsula, Japan. *Sediment. Geol.* 80, 67–75. [https://doi.org/10.1016/0037-0738\(92\)90032-M](https://doi.org/10.1016/0037-0738(92)90032-M).
- Ito, M., Nishida, N., Otake, S., Saito, T., Okazaki, H., Nishikawa, T., 2006a. Glacioeustatic signals and sequence architecture of the Pliocene–Pleistocene forearc basin-fill successions on the Boso Peninsula, central Japan. In: Ito, M., Yagishita, K., Ikehara, K., Matsuda, H. (Eds.), *Field Excursion Guidebook, 17th International Sedimentological Congress, Fukuoka, Japan*. Sedimentological Society of Japan, FE-a4, pp. 1–30.
- Ito, M., Takao, A., Ishikawa, K., Himeno, O., 2006b. A new avenue of sedimentological study of deep-water successions: reorganization of the lowstand depositional model. *Jour. Jpn. Assoc. Pet. Technol.* 71, 21–33 (in Japanese with English abstract).
- Japan Meteorological Agency. Daily and every 3-hours meteorological data at the ground surface (1981–2010). <http://www.jma.go.jp/jma/indexe.html>
- Jonkers, L., Brummer, G.-J.A., Peeters, F.J.C., van Aken, H.M., De Jong, M.F., 2010. Seasonal stratification, shell flux, and oxygen isotope dynamics of left-coiling *N. pachyderma* and *T. quinqueloba* in the western subpolar North Atlantic. *Paleoceanography* 25, PA2204 doi: 2210.1002/palo.20018.
- Jonkers, L., Reynolds, C.E., Richey, J., Hall, I.R., 2015. Lunar periodicity in the shell flux of planktonic foraminifera in the Gulf of Mexico. *Biogeosciences* 12, 3061–3070. <https://doi.org/10.5194/bg-12-3061-2015>.
- Jouzel, J., Masson-Delmotte, V., Cattani, O., Dreyfus, G., Falourd, S., Hoffmann, G., Minster, B., Nouet, J., Barnola, J.M., Chappellaz, J., Fischer, H., Gallet, J.C., Johnsen, S., Leuenberger, M., Loulergue, L., Luethi, D., Oerter, H., Parrenin, F., Raisbeck, G., Raynaud, D., Schilt, A., Schwander, J., Selmo, E., Souchez, R., Spahni, R., Stauffer, B., Steffensen, J.P., Stenni, B., Stocker, T.F., Tison, J.L., Werner, M., Wolff, E.W., 2007. Orbital and millennial Antarctic climate variability over the past 800,000 years. *Science* 317, 793–796. <https://doi.org/10.1126/science.1141038>.
- Kamemaru, A., 1996. Biostratigraphy of the Chiba section of the Boso Peninsula toward establishing the lower–middle Pleistocene boundary stratotype based on benthic foraminiferal evidence. In: *Proceedings on the Research of Stratotype for the Lower–Middle Pleistocene Boundary*. Intern. Res. Group Lower–Middle, Middle–Upper Pleistocene Bound. Jpn. Assoc. Quat. Res. pp. 46–54.
- Kameo, K., Haneda, Y., Kubota, Y., Suganuma, Y., Okada, M., 2017. Biostratigraphy of calcareous nannofossils and inferred sea surface conditions around the Matuyama-Brunhes Boundary of the Kokumoto Formation, Kazusa Group, distributed in the Boso Peninsula, central Japan (poster session). In: *Abstracts, Japan Geoscience Union Meeting, 2017, SGL38–p04, Japan Geoscience Union*.
- Kameo, K., Okada, M., El-Masry, M., Hisamitsu, T., Saito, S., Nakazato, H., Ohkouchi, N., Ikehara, M., Yasuda, H., Kitazato, H., Taira, A., 2006. Age model, physical properties and paleoenvironmental implications of the middle Pleistocene core sediments in the Choshi area, central Japan. *Island. Arc* 15, 366–377. <https://doi.org/10.1111/j.1440-1738.2006.00535.x>.
- Kameo, K., Watanabe, K., Haneda, Y., Okada, M., Suganuma, Y., 2016. Calcareous nannofossil biostratigraphy and estimated sea surface environment around the Matuyama-Brunhes geomagnetic polarity reversal from the Kokumoto Formation in the Boso Peninsula (poster session). In: *Abstracts with Programs, 166th Regular Meeting, Palaeontological Society of Japan, 2016, 39, Palaeontological Society of Japan*.
- Kariya, C., Hyodo, M., Tanigawa, K., Sato, H., 2010. Sea-level variation during MIS 11 constrained by stepwise Osaka Bay extensions and its relation with climatic evolution. *Quat. Sci. Rev.* 29, 1863–1879. <https://doi.org/10.1016/j.quascirev.2010.04.005>.
- Katsura, Y., 1984. Depositional environments of the Plio-Pleistocene Kazusa Group, Boso Peninsula, Japan. In: *Science Reports of the Institute of Geoscience, University of Tsukuba, Section B, Geological Sciences, vol. 5, pp. 69–104*.
- Kazaoka, O., Suganuma, Y., Okada, M., Kameo, K., Head, M.J., Yoshida, T., Kameyama, S., Nirei, H., Aida, N., Kumai, H., 2015. Stratigraphy of the Kazusa Group, Central Japan: a high-resolution marine sedimentary sequence from the Lower to Middle Pleistocene. *Quat. Int.* 383, 116–135. <https://doi.org/10.1016/j.quaint.2015.02.065>.
- Kitaba, I., Harada, M., Hyodo, M., Katoh, S., Sato, H., Matsushita, M., 2011. MIS 21 and the Mid-Pleistocene climate transition: climate and sea-level variation from a sediment core in Osaka Bay. *Jpn. Palaeogeogr. Palaeoclimatol. Palaeoecol.* 299, 227–239. <https://doi.org/10.1016/j.palaeo.2010.11.004>.
- Kitaba, I., Hyodo, M., Katoh, S., Dettman, D.L., Sato, H., 2013. Midlatitude cooling caused by geomagnetic field minimum during polarity reversal. *PNAS* 110, 1215–1220. <https://doi.org/10.1073/pnas.1213389110/-DCSupplemental>.
- Kitaba, I., Hyodo, M., Nakagawa, T., Katoh, S., Dettman, D.L., Sato, H., 2017. Geological support for the Umbrella Effect as a link between geomagnetic field and climate. *Sci. Rep.* 7, 40682. <https://doi.org/10.1038/srep40682>.
- Kitaba, I., Iwabe, C., Hyodo, M., Katoh, S., Matsushita, M., 2009. High-resolution climate stratigraphy across the Matuyama-Brunhes transition from palynological data of Osaka Bay sediments in southwestern Japan. *Palaeogeogr. Palaeoclimatol. Palaeoecol.* 272, 115–123. <https://doi.org/10.1016/j.palaeo.2008.11.013>.
- Kitaba, I., Hyodo, M., Katoh, S., Matsushita, M., 2012. Phase-lagged warming and the disruption of climatic rhythms during the Matuyama-Brunhes magnetic

- polarity transition. *Gondwana Res.* 21, 595–600. <https://doi.org/10.1016/j.jgr.2011.07.005>.
- Kruglikova, S.B., 1969. Radiolarians in the surface layer of the sediments of the northern half of the Pacific Ocean. In: Kort, P.P. (Ed.), *The Pacific Ocean, Microflora and Microfauna in the Recent of Pacific Ocean*. Nauka, Moscow, pp. 48–72 (in Russian).
- Kubota, Y., Kimoto, K., Tada, R., Oda, H., Yokoyama, Y., Matsuzaki, H., 2010. Variations of East Asian summer monsoon since the last deglaciation based on Mg/Ca and oxygen isotope of planktic foraminifera in the northern East China Sea. *Paleoceanography* 25, PA4205. <https://doi.org/10.1029/2009PA001891>.
- Kuroyanagi, A., Kawahata, H., 2004. Vertical distribution of living planktonic foraminifera in the seas around Japan. *Mar. Micropaleontol.* 53, 173–196. <https://doi.org/10.1016/j.marmicro.2004.06.001>.
- Lang, N., Wolff, E.W., 2011. Interglacial and glacial variability from the last 800 ka in marine, ice and terrestrial archives. *Clim. Past.* 7, 361–380. <https://doi.org/10.5194/cp-7-361-2011>.
- Layer, P.W., 2000. Argon-40/argon-39 age of the El'gygytgyn impact event, Chukotka, Russia. *Meteorit. Planet. Sci.* 35, 591–599. <https://doi.org/10.1111/j.1945-5100.2000.tb01439.x>.
- LePage, B.A., Yang, H., Matsumoto, M., 2005. The evolution and biogeographic history of *Metasequoia*. In: LePage, B.A., Williams, C.J., Yang, H. (Eds.), *The Geobiology and Ecology of Metasequoia*. Springer, Dordrecht, pp. 3–114.
- Lisiecki, L.E., Raymo, M.E., 2005. A Pliocene-Pleistocene stack of 57 globally distributed benthic $\delta^{18}\text{O}$ records. *Paleoceanography* 20. <https://doi.org/10.1029/2004PA001071>. PA1003.
- Liu, Q., Jin, C., Hu, P., Jiang, Z., Ge, K., Roberts, A.P., 2015. Magnetostratigraphy of Chinese loess–paleosol sequences. *Earth-Science Rev.* 150, 139–167. <https://doi.org/10.1016/j.earscirev.2015.07.009>.
- Locarnini, R.A., Mishonov, A.V., Antonov, J.I., Boyer, T.P., Garcia, H.E., Baranova, O.K., Zweng, M.M., Paver, C.R., Reagan, J.R., Johnson, D.R., Hamilton, M., Seidov, D., 2013. *World Ocean Atlas 2013, volume 1: Temperature*. In: Levitus, S. (Ed.), *A Mishonov Technical Ed.; NOAA Atlas NESDIS 73*, 40 pp.
- Maasch, K.A., 1988. Statistical detection of the mid-Pleistocene transition. *Clim. Dyn.* 2, 133–143.
- Maiorano, P., Bertini, A., Capolongo, D., Eramo, G., Gallicchio, S., Girona, A., Pinto, D., Toti, F., Venturi, G., Marino, M., 2016. Climate signatures through Marine Isotope Stage 19 in the Montalbano Jonico section (southern Italy): a land–sea perspective. *Paleogeogr. Palaeoclimatol. Palaeoecol.* 461, 341–361. <https://doi.org/10.1016/j.palaeo.2016.08.029>.
- Marino, M., Bertini, A., Ciaranfi, N., Aiello, G., Barra, D., Gallicchio, S., Girona, A., La Perna, R., Lirer, F., Maiorano, P., Petrosino, P., Toti, F., 2015. Paleoenvironmental and climatostatigraphic insights for Marine Isotope Stage 19 (Pleistocene) at the Montalbano Jonico succession, South Italy. *Quat. Int.* 383, 104–115. <https://doi.org/10.1016/j.quaint.2015.01.043>.
- Matsuoka, H., Okada, H., 1990. Time-progressive morphometric changes of the genus *Gephyrocapsa* in the Quaternary sequence of the tropical Indian Ocean, Site 709. In: Dundan, R.A., Backman, J., Peterson, L.C., et al. (Eds.), *Proc. ODP, Sci. Res.*, 115: College Station, TX, pp. 255–270 (Ocean Drilling Program).
- Matsuzaki, K.M., Itaki, T., 2017. New northwest Pacific radiolarian data as a tool to estimate past sea surface and intermediate water temperatures. *Paleoceanography* 32, 218–245. <https://doi.org/10.1002/2017PA003087>.
- Mitsunashi, T., Yasukuni, N., Shinada, Y., 1959. Stratigraphical section of the Kazusa Group along the shores of the rivers Yoro and Obitsu. *Bull. Geol. Surv. Jpn.* 10, 83–98 (in Japanese).
- Mitsunashi, T., Yazaki, K., Kageyama, K., Shimada, T., Ono, E., Yasukuni, N., Makino, T., Shinada, Y., Fujiwara, K., Kamata, S., 1961. Geological maps of the oil and gas field of Japan no. 4, Futtsu-Otaki, 1:50,000. Geological Survey of Japan.
- Momohara, A., 2005. Paleogeology and history of *Metasequoia* in Japan, with reference to its extinction and survival in East Asia. In: LePage, B.A., Williams, C.J., Yang, H. (Eds.), *The Geobiology and Ecology of Metasequoia*. Springer, Dordrecht, pp. 115–136.
- Moore Jr., T.C., Burckle, L.H., Geitzenauer, K., Luz, B., Molina-Cruz, A., Robertson, J.H., Sachs, H., Sancetta, C., Thiede, J., Thompson, P., Wenkam, C., 1980. The reconstruction of sea surface temperatures in the Pacific Ocean of 18,000 B.P. *Mar. Micropaleontol.* 5, 215–247. [https://doi.org/10.1016/0377-8398\(80\)90012-2](https://doi.org/10.1016/0377-8398(80)90012-2).
- Motoyama, I., Itaki, T., Kamikuri, S., Taketani, Y., Okada, M., 2017. Cenozoic biostratigraphy, chronostratigraphy and paleoceanography in the Boso Peninsula and Bandai Volcano in the Aizu region, East Japan. *Sci. Rep. Niigata Univ. Geol.* 32 (Suppl. ment), 1–27.
- Mudelsee, M., Schulz, M., 1997. The Mid-Pleistocene climate transition: onset of 100 ka cycle lags ice volume build-up by 280 ka. *Earth Planet. Sci. Lett.* 151, 117–123. [https://doi.org/10.1016/S0012-821X\(97\)00114-3](https://doi.org/10.1016/S0012-821X(97)00114-3).
- Mudelsee, M., Statterger, K., 1997. Exploring the structure of the mid-Pleistocene revolution with advanced methods of time-series analysis. *Geol. Rundsch.* 86, 499–511. <https://doi.org/10.1007/s005310050157>.
- Nakagawa, T., Tarasov, P.E., Nishida, K., Gotanda, K., Yasuda, Y., 2002. Quantitative pollen-based climate reconstruction in central Japan: application to surface and Late Quaternary spectra. *Quat. Sci. Rev.* 21, 2099–2113. [https://doi.org/10.1016/S0277-3791\(02\)00014-8](https://doi.org/10.1016/S0277-3791(02)00014-8).
- Nakamura, K., Takao, A., Ito, M., 2007. Geometry and internal organization of hyperpycnites associated with a shelf-margin delta, the Middle Pleistocene Kokumoto Formation on the Boso Peninsula of Japan. *J. Sedimentological Soc. Jpn.* 64, 65–68 (in Japanese with English abstract).
- Nakanishi, S., Ohba, T., Takeda, Y., Hattori, T., 1983. Illustration of Vegetation in Japan Vol. I for. Veg. 208 pp., Hoikusha, Osaka (in Japanese).
- Nakazato, H., Sato, H., Okuda, M., CHOSHI core research group, 2003. Tephrostratigraphy of a 250 m core from the Inubo Group in the northeast part of Chiba Prefecture. In: Abstracts of the 110th Annual Meeting of the Geological Society of Japan, P. 3. Geological Society of Japan, Shizuoka (in Japanese).
- Nanayama, F., Nakazato, H., Ooi, S., Nakajima, R., 2016. Geological map of Japan 8–77. Mobarai 1, 50,000. Geological Survey of Japan.
- Naya, T., Yamaguchi, M., Mizuno, K., 2009. Occurrence horizons of diatom fossils and recognition of marine sediments in the Shobu Core (GS-SB-1), Saitama Prefecture, central Kanto plain, Japan. *Bull. Geol. Surv. Jpn.* 60, 245–256 (in Japanese with English abstract).
- Nigrini, C., 1970. Radiolarian assemblages in the North Pacific and their application to a study of Quaternary sediments in core V20-130. In: Hays, J.D. (Ed.), *Geological Investigations of the North Pacific*. The Geological Society of America, Inc., Memoir, vol. 126, pp. 130–183.
- Niimura, Y., Irino, T., Oba, T., 2006. Paleoenvironmental changes off Kashima of central Japan during the last 144,000 years based on planktonic foraminiferal assemblage. *Fossils (The Palaeontological Society of Japan)* 79, 4–17 (in Japanese with English abstract).
- Niitsuma, N., 1976. Magnetic stratigraphy in the Boso Peninsula. *Jour. Geol. Soc. Japan* 82, 163–181 (in Japanese with English abstract).
- Nirei, H., Kusuda, T., Kazaoka, O., Tanaka, H., Umetsu, K., 1989. Geological Map of Chiba 1:100,000. Policy and Planning Department of Chiba Prefecture.
- Nirei, H., Kusuda, T., Mitsunashi, T., Kikuchi, T., 1987. Stratigraphic studies of the Pleistocene in the Boso Peninsula facing the Pacific, Central Japan. In: Ithara, M., Kamei, T. (Eds.), *Proceedings of the First International Colloquium on Quaternary Stratigraphy of Asia and Pacific Area*. INQUA Commission on Quaternary Stratigraphy, Osaka, pp. 32–42.
- Nishida, N., Kazaoka, O., Izumi, K., Suganuma, Y., Okada, M., Yoshida, T., Ogitsu, I., Nakazato, H., Kameyama, S., Kagawa, A., Morisaki, M., Nirei, H., 2016. Sedimentary processes and depositional environments of a continuous marine succession across the Lower–Middle Pleistocene boundary: Kokumoto Formation, Kazusa group, central Japan. *Quat. Int.* 397, 3–15. <https://doi.org/10.1016/j.quaint.2015.06.045>.
- Oba, T., Hattori, T., 1992. Living planktonic foraminiferal assemblages at the Japan trench off Boso Peninsula. *Fossils (The Palaeontological Society of Japan)* 52, 12–19 (in Japanese with English abstract).
- Oba, T., Irino, T., Yamamoto, M., Murayama, M., Takamura, A., Aoki, K., 2006. Paleoenvironmental change off central Japan since the last 144,000 years based on high-resolution oxygen and carbon isotope records. *Glob. Planet. Change* 53, 5–20. <https://doi.org/10.1016/j.gloplacha.2006.05.002>.
- Oda, M., 1977. Planktonic foraminiferal biostratigraphy of the late Cenozoic sedimentary sequence, central Honshu. *Japan Sci. Rep. Tohoku Univ., 2nd Ser. (Geol.)* 48 (1), 1–72.
- Oda, M., Ishizaki, K., Takayanagi, Y., 1983. Analysis of planktic foraminifera in the marine surface sediments of east of Honshu. Special Project Research “The Ocean Characteristics and their Changes”. Newsletter 11, 3–11.
- Ogg, J., Ogg, G., Gradstein, F., 2016. *A Concise Geologic Time Scale: 2016*. Elsevier, 240 pp.
- Okada, H., Honjo, S., 1973. The distribution of oceanic coccolithophorids in the Pacific. *Deep-Sea Research* 20, 335–374. [https://doi.org/10.1016/0011-7471\(73\)90059-4](https://doi.org/10.1016/0011-7471(73)90059-4).
- Okada, M., Niitsuma, N., 1989. Detailed paleomagnetic records during the Brunhes–Matuyama geomagnetic reversal and a direct determination of depth lag for magnetization in marine sediments. *Phys. Earth Planet. Int.* 56, 133–150. [https://doi.org/10.1016/0031-9201\(89\)90043-5](https://doi.org/10.1016/0031-9201(89)90043-5).
- Okada, M., Suganuma, Y., Haneda, Y., Kazaoka, O., 2017. Paleomagnetic direction and paleointensity variations during the Matuyama–Brunhes polarity transition from a marine succession in the Chiba composite section of the Boso Peninsula, central Japan. *Earth, Planets, Space* 69 (45). <https://doi.org/10.1186/s40623-017-0627-1>.
- Okuda, M., Nakazato, H., Miyoshi, N., Nakagawa, T., Okazaki, H., Saito, S., Taira, A., 2006. MIS11–19 pollen stratigraphy from the 250-m Choshi core, northeast Boso Peninsula, central Japan: implications for the early/mid-Brunhes (400–780 ka) climate signals. *Island Arc* 15, 338–354. <https://doi.org/10.1111/j.1440-1738.2006.00533.x>.
- Onishi, I., 1969. Pollen flora of the Kazusa Group in the Boso Peninsula, Japan. *Earth Science (Chikyu Kagaku)* 24, 222–224 (in Japanese with English abstract).
- Ozaki, H., 1958. Stratigraphical and paleontological studies on the Neogene and Pleistocene formations of the Choshi district. *Bulletin of the National Museum (Tokyo)* 4, 1–182.
- Parente, A., Cachão, M., Baumann, K.-H., de Abreu, L., Ferreira, J., 2004. Morphometry of *Coccolithus* s.l. (Coccolithophore, Haptophyta) from offshore Portugal, during the last 200 kyr. *Micropaleontology* 50, 107–120.
- Pickering, K.T., Souter, C., Oba, T., Taira, A., Schaaf, M., Platzman, E., 1999. Glacio-eustatic control on deep-marine clastic forearc sedimentation, Pliocene–mid-Pleistocene (c. 1180–600 ka) Kazusa Group. *SE Japan. Jour. Geol. Soc. London* 156, 125–136.
- Pol, K., Masson-Delmotte, V., Johnsen, S., Bigler, M., Cattani, O., Durand, G., Falourd, S., Jouzel, J., Minster, B., Parrenin, F., Ritz, C., Steen-Larsen, H.C., Stenni, B., 2010. New MIS 19 EPICA Dome C high resolution deuterium data Hints for a problematic preservation of climate variability at sub-millennial scale in the “oldest ice”. *Earth Planet. Sci. Lett.* 298, 95–103. <https://doi.org/10.1016/j.epsl.2010.07.030>.
- Prokopenko, A.A., Hinnov, L.A., Williams, D.F., Kuzmin, M.I., 2006. Orbital forcing of continental climate during the Pleistocene: a complete astronomically tuned

- climatic record from Lake Baikal, SE Siberia. *Quat. Sci. Rev.* 25, 3431–3457. <https://doi.org/10.1016/j.quascirev.2006.10.002>.
- Railsback, L.B., Gibbard, P.L., Head, M.J., Voarintsoa, N.R.G., Toucanne, S., 2015. An optimized scheme of lettered marine isotope substages for the last 1.0 million years, and the climatostratigraphic nature of isotope stages and substages. *Quat. Sci. Rev.* 111, 94–106. <https://doi.org/10.1016/j.quascirev.2015.01.012>.
- Raymo, M.E., Oppo, D.W., Curry, W., 1997. The Mid-Pleistocene climate transition: a deep sea carbon isotopic perspective. *Paleoceanography* 12, 546–559. <https://doi.org/10.1029/97PA01019>.
- Rio, D., 1982. The fossil distribution of coccolithophore genus *Gephyrocapsa* Kamptner and related Plio-Pleistocene chronostratigraphic problems. In: *Prell, W.L., Gardner, J.V., et al. (Eds.), Int. Repts. DSDP, 68: Washington (U.S. Govt. Printing Office)*, pp. 325–343.
- Rodríguez-Tovar, F.J., Dorador, J., 2014. Ichnological analysis of Pleistocene sediments from the IODP Site U1385 “Shackleton site” on the Iberian margin: Approaching paleoenvironmental conditions. *Palaeogeogr. Palaeoclimatol. Palaeoecol.* 409, 24–32. <https://doi.org/10.1016/j.palaeo.2014.04.027>.
- Sagnotti, L., Giaccio, B., Liddicoat, J.C., Nomade, S., Renne, P.R., Scardia, G., Sprain, C.J., 2010. How fast was the Matuyama–Brunhes geomagnetic reversal? A new subcentennial record from the Sulmona Basin, central Italy. *Geophys. J. Int.* 204, 798–812. <https://doi.org/10.1093/gji/ggv486>.
- Sato, T., Takayama, T., Kato, M., Kudo, T., Kameo, K., 1988. Calcareous microfossil biostratigraphy of the uppermost Cenozoic formations distributed in the coast of the Japan Sea, Part 4: Conclusion. *Jour. Japan. Asso. Pet. Technol.* 53, 474–491 (in Japanese with English abstract).
- Satoguchi, Y., 1995. Tephrostratigraphy in the lower to middle Kazusa Group in the Boso Peninsula. *Japan. Jour. Geol. Soc. Japan* 101, 767–782 (in Japanese with English abstract).
- Schiebel, R., Wanek, J., Bork, M., Hemleben, C., 2001. Planktic foraminiferal production stimulated by chlorophyll redistribution and entrainment of nutrients. *Deep-Sea Research* 1 48, 721–740. [https://doi.org/10.1016/S0967-0637\(00\)00065-0](https://doi.org/10.1016/S0967-0637(00)00065-0).
- Schlitzer, R., 2015. Ocean Data view. <http://odv.awi.de>.
- Seno, T., Takano, T., 1989. Seismotectonics at the trench-trench-trench triple junction off Central Honshu. *Pure and Applied Geophysics* 129, 27–40. <https://doi.org/10.1007/BF00874623>.
- Shackleton, N.J., Sánchez-Goni, M.F., Pailler, D., Lancelot, Y., 2003. Marine Isotope Substage 5e and the Eemian Interglacial. *Glob. Planet. Change* 36, 151–155. [https://doi.org/10.1016/S0921-8181\(02\)00181-9](https://doi.org/10.1016/S0921-8181(02)00181-9).
- Simon, Q., Bourlès, D.L., Bassinot, F., Nomade, S., Marino, M., Ciaranfi, N., Girone, A., Maiorano, P., Thouveny, N., Choy, S., Dewilde, F., Scao, V., Isguder, G., Blamart, D., 2017. Authigenic $^{10}\text{Be}/^{9}\text{Be}$ ratio signature of the Matuyama–Brunhes boundary in the Montalbano Jonico marine succession. *Earth Planet. Sci. Lett.* 460, 255–267. <https://doi.org/10.1016/j.epsl.2016.11.052>.
- Simon, Q., Thouveny, N., Bourlès, D.L., Bassinot, F., Savranskaia, T., Valet, J.-P., Team, A.S.T.E.R., 2018. Increased production of cosmogenic ^{10}Be recorded in oceanic sediment sequences: information on the age, duration, and amplitude of the geomagnetic dipole moment minimum over the Matuyama–Brunhes transition. *Earth Planet. Sci. Lett.* 489, 191–202. <https://doi.org/10.1016/j.epsl.2018.02.036>.
- Spindler, M., Hemleben, C., Bayer, U., Bé, A., Anderson, O., 1979. Lunar periodicity of reproduction in the planktonic foraminifer *Hastigerina pelagica*. *Mar. Ecol.-Prog. Ser.* 1, 61–64.
- Stocker, T.F., Johnsen, S.J., 2003. A minimum thermodynamic model for the bipolar seesaw. *Paleoceanography* 18 (4), 1087. <https://doi.org/10.1029/2003PA000920>.
- Suganuma, Y., Okada, M., Horie, K., Kaiden, H., Takehara, M., Senda, R., Kimura, J., Haneda, Y., Kawamura, K., Kazaoka, O., Head, M.J., 2015. Age of Matuyama–Brunhes boundary constrained by U–Pb zircon dating of a wide-spread tephra. *Geology* 43, 491–494. <https://doi.org/10.1130/G36625.1>.
- Suganuma, Y., Okuno, J., Heslop, D., Roberts, A.P., Yamazaki, T., Yokoyama, Y., 2011. Post-depositional remanent magnetization lock-in for marine sediments deduced from ^{10}Be and paleomagnetic records through the Matuyama–Brunhes boundary. *Earth Planet. Sci. Lett.* 311, 39–52. <https://doi.org/10.1016/j.epsl.2011.08.038>.
- Suganuma, Y., Yokoyama, Y., Yamazaki, T., Kawamura, K., Horng, C.S., Matsuzaki, H., 2010. ^{10}Be evidence for delayed acquisition of remanent magnetization in marine sediments: implication for a new age for the Matuyama–Brunhes boundary. *Earth Planet. Sci. Lett.* 296, 443–450. <https://doi.org/10.1016/j.epsl.2010.05.031>.
- Sun, Y., An, Z., Clemens, S.C., Bloemendal, J., Vandenbergh, J., 2010. Seven million years of wind and precipitation variability on the Chinese Loess Plateau. *Earth Planet. Sci. Lett.* 297, 525–535. <https://doi.org/10.1016/j.epsl.2010.07.004>.
- Sun, Y.B., Clemens, S.C., An, Z.S., Yu, Z.W., 2006. Astronomical timescale and palaeoclimatic implication of stacked 3.6-Myr monsoon records from the Chinese Loess Plateau. *Quat. Sci. Rev.* 25, 33–48. <https://doi.org/10.1016/j.quascirev.2005.07.005>.
- Suzuki, T., Eden, D., Danbara, T., Fujiwara, O., 2005. Correlation of the Hakkoda-Kokumoto tephra, a widespread Middle Pleistocene tephra erupted from the Hakkoda Caldera, northeast Japan. *Island Arc* 14, 666–678. <https://doi.org/10.1111/j.1440-1738.2005.00475.x>.
- Svensmark, H., Friis-Christensen, E., 1997. Variation of cosmic ray flux and global cloud coverage – a missing link in solar-climate relationships. *J. Atmos. Solar-Terrest. Phys.* 59, 1225–1232. [https://doi.org/10.1016/S1364-6826\(97\)00001-1](https://doi.org/10.1016/S1364-6826(97)00001-1).
- Tai, A., 1973. A study on the pollen stratigraphy of the Osaka Group, Plio-Pleistocene deposits in the Osaka basin. *Mem. Fac. Sci., Kyoto Univ. Geol. & Min* 39, 123–165.
- Takemoto, A., Oda, M., 1997. New planktic foraminiferal transfer functions for the Kuroshio-Oyashio current region off Japan. *Paleontological Research* 1, 291–310. <https://doi.org/10.2517/prpsj.1.291>.
- Takehita, Y., Matsushima, N., Teradaira, H., Uchiyama, T., Kumai, H., 2016. A marker tephra bed close to the Middle Pleistocene boundary: distribution of the Ontake-Byakubi tephra in central Japan. *Quat. Int.* 397, 27–38. <https://doi.org/10.1016/j.quaint.2015.03.054>.
- Tanaka, S., Takahashi, K., 2008. Detailed vertical distribution of radiolarian assemblage (0–3000 m, fifteen layers) in the central subarctic Pacific, June 2006. *Mem. Fac. Kyushu Univ., Ser. D, Earth Planet. Sci.* 32, 49–72.
- Thompson, P.R., Shackleton, N.J., 1980. North Pacific palaeoceanography: late Quaternary coiling variations of planktonic foraminifer *Neogloboquadrina pachyderma*. *Nature* 287, 829–833. <https://doi.org/10.1038/287829a0>.
- Toti, F., 2015. Interglacial vegetation patterns at the early-middle Pleistocene transition: a point of view from the Montalbano Jonico section (Southern Italy). *Alp. Mediterr. Quat.* 28, 131–143.
- Tsuji, T., Miyata, Y., Okada, M., Mita, I., Nakagawa, H., Sato, Y., Nakamizu, M., 2005. High-resolution chronology of the lower Pleistocene Otadai and Umegase formations of the Kazusa Group, Boso Peninsula, central Japan: chronostratigraphy of the JNOC TR-3 cores based on oxygen isotope, magnetostratigraphy and calcareous nannofossil. *Jour. Geol. Soc. Japan* 111, 1–20 (in Japanese with English abstract).
- Tsunakawa, H., Okada, M., Niitsuma, N., 1999. Further application of the deconvolution method of post-depositional DRM to the precise record of the Matuyama–Brunhes reversal in the sediments from the Boso Peninsula. *Japan. Earth Planets Space* 51, 169–173. <https://doi.org/10.1186/BF03352221>.
- Tzedakis, P.C., 2010. The MIS 11 – MIS 1 analogy, southern European vegetation, atmospheric methane and the “early anthropogenic hypothesis”. *Clim. Past* 6, 131–144. <https://doi.org/10.5194/cp-6-131-2010>.
- Tzedakis, P.C., Channell, J.E.T., Hodell, D.A., Kleiven, H.F., Skinner, L.C., 2012. Determining the natural length of the current interglacial. *Nature Geoscience* 5, 138–142. <https://doi.org/10.1038/ngeo1358>.
- Uchida, M., Ohkushi, K., Kimoto, K., Inagaki, F., Ishimura, T., Tsunogai, U., TuZino, T., Shibata, Y., 2008. Radiocarbon-based carbon source quantification of anomalous isotopic foraminifera in last glacial sediments in the western North Pacific. *Geochemistry, Geophys. Geosystems* 9. <https://doi.org/10.1029/2006GC001558>.
- Uchman, A., Wetzel, A., 2012. Deep-sea fans. In: *Knaust, D., Bromley, R.G. (Eds.), Trace Fossils as Indicators of Sedimentary Environments. Developments in Sedimentology*, vol. 64, pp. 643–672.
- Ueki, T., Yamaguchi, M., Hongo, M., Naya, T., Mizuno, K., 2009. Paleomagnetic and rock-magnetic measurements of the GS-SB-1 core at Shobu Town, central Kanto Plain, Japan. *Bull. Geol. Surv. Japan* 60, 199–243 (in Japanese with English abstract).
- Valet, J.P., Bassinot, F., Bouilloux, A., Bourlès, D., Nomade, S., Guillou, V., Lopes, F., Thouveny, N., Dewilde, F., 2014. Geomagnetic, cosmogenic and climatic changes across the last geomagnetic reversal from Equatorial Indian Ocean sediments. *Earth Planet. Sci. Lett.* 397, 67–79. <https://doi.org/10.1016/j.epsl.2014.03.053>.
- Vincent, E., Berger, W.H., 1981. Planktonic foraminifera and their use in paleoceanography. In: *Emiliani, C. (Ed.), The Oceanic Lithosphere: the Sea, Vol. 7, Wiley-Interscience, New York*, pp. 1025–1119.
- Wennrich, V., Andreev, A.A., Tarasov, P.E., Fedorov, G., Zhao, W., Gebhardt, C.A., Meyer-Jacob, C., Snyder, J.A., Nowaczyk, N.R., Schwamborn, G., Chaplignin, B., Anderson, P.M., Lozhkin, A.V., Minyuk, P.S., Koeberl, C., Melles, M., 2016. Impact processes, permafrost dynamics, and climate and environmental variability in the terrestrial Arctic as inferred from the unique 3.6 Myr record of Lake El'gygytgyn, Far East Russia – a review. *Quat. Sci. Rev.* 147, 221–244. <https://doi.org/10.1016/j.quascirev.2016.03.019>.
- Wennrich, V., Minyuk, P.S., Borkhodoev, V., Francke, A., Ritter, B., Nowaczyk, N.R., Sauerbrey, M.A., Brigham-Grette, J., Melles, M., 2014. Pliocene to Pleistocene climate and environmental history of Lake El'gygytgyn, Far East Russian Arctic, based on high-resolution inorganic geochemistry data. *Clim. Past* 10, 1381–1399. <https://doi.org/10.5194/cp-10-1381-2014>.
- Wetzel, A., Uchman, A., 2012. Hemipelagic and pelagic basin plains. In: *Knaust, D., Bromley, R.G. (Eds.), Trace Fossils as Indicators of Sedimentary Environments. Developments in Sedimentology*, vol. 64, pp. 673–702.
- Yamamoto, M., Suemune, R., Oba, T., 2005. Equatorward shift of the subarctic boundary in the northwestern Pacific during the last deglaciation. *Geophys. Res. Lett.* 32, 1–4. <https://doi.org/10.1029/2004GL021903>.
- Yin, Q.Z., Berger, A., 2012. Individual contribution of insolation and CO₂ to the interglacial climates of the past 800,000 years. *Clim. Dyn.* 38, 709–724. <https://doi.org/10.1007/s00382-011-1013-5>.
- Yoshioka, K., 1973. *Plant Geography*. Kyoritsu-Shuppan Publishing House, Tokyo, 84 pp (in Japanese).
- Zhang, Y., Huang, D., 2011. Has the East Asian westerly jet experienced a poleward displacement in recent decades? *Adv. Atmos. Sci.* 28, 1259–1265. <https://doi.org/10.1007/s00376-011-9185-9>.

Update

Quaternary Science Reviews

Volume 204, Issue , 15 January 2019, Page 220–221

DOI: <https://doi.org/10.1016/j.quascirev.2018.11.026>



Corrigendum

Corrigendum to “Paleoclimatic and paleoceanographic records through Marine Isotope Stage 19 at the Chiba composite section, central Japan: A key reference for the Early–Middle Pleistocene Subseries boundary” [Quat. Sci. Rev. 191 (2018) 406–430][☆]



Yusuke Suganuma ^{a, b, *}, Yuki Haneda ^c, Koji Kameo ^d, Yoshimi Kubota ^e, Hiroki Hayashi ^f, Takuya Itaki ^g, Masaaki Okuda ^h, Martin J. Head ⁱ, Manami Sugaya ^j, Hiroomi Nakazato ^k, Atsuo Igarashi ^l, Kizuku Shikoku ^f, Misao Hongo ^m, Masami Watanabe ⁿ, Yasufumi Satoguchi ^o, Yoshihiro Takeshita ^p, Naohisa Nishida ^q, Kentaro Izumi ^r, Kenji Kawamura ^{a, b}, Moto Kawamata ^b, Jun'ichi Okuno ^{a, b}, Takeshi Yoshida ^s, Itaru Ogitsu ^s, Hisashi Yabusaki ^s, Makoto Okada ^c

^a National Institute of Polar Research, 10-3 Midori-cho, Tachikawa, Tokyo, 190-8518, Japan

^b Department of Polar Science, School of Multidisciplinary Sciences, The Graduate University for Advanced Studies (SOKENDAI), Midori-cho 10-3, Tachikawa, Tokyo, 190-8518, Japan

^c Department of Earth Sciences, Ibaraki University, 2-2-1 Bunkyo, Mito, Ibaraki, 310-8512, Japan

^d Department of Earth Sciences, Chiba University, 1-33 Yayoi, Inage, Chiba, Chiba, 263-8522, Japan

^e Department of Geology and Paleontology, National Museum of Nature and Science, 4-1-1 Amakubo, Tsukuba, Ibaraki, 305-0005, Japan

^f Interdisciplinary Graduate School of Science and Engineering, Shimane University, Nishikawatsucho 1060, Matsue, Shimane, 690-8504, Japan

^g Geological Survey of Japan, AIST, Tsukuba Central 7, 1-1-1 Higashi, Tsukuba, Ibaraki, 305-8567, Japan

^h Natural History Museum and Institute, Chiba, 955-2 Aoba-cho, Chuo, Chiba, 260-8682, Japan

ⁱ Department of Earth Sciences, 1812 Sir Isaac Brock Way, Brock University, Ontario, L2S 3A1, Canada

^j Giken Consul., Ltd., 1-15-3 Shimokoide, Maebashi, Gunma, 371-0031, Japan

^k Institute for Rural Engineering, NARO, 2-1-6 Kannondai, Tsukuba, Ibaraki, 305-8609, Japan

^l Fukken Co., Ltd. Tokyo Branch Office, 3-8-15 Iwamoto-cho, Chiyoda, Tokyo, 101-0032, Japan

^m Alps Technical Research Laboratory Co., Ltd., 2287-27 Toyoshina-takibe, Azumino, Nagano, 399-8204, Japan

ⁿ Archaeological Research Consultant, Inc., 131 Shimohigashikawatsu, Matsue, 690-0822, Japan

^o Lake Biwa Museum, 1091 Oroshimo-cho, Kusatsu, 525-0001, Japan

^p Institute of Education, Shinshu University, 6-ro Nishinagano, Nagano 380-8544, Japan

^q Department of Environmental Sciences, Tokyo Gakugei University, 4-1-1 Nukuikita, Koganei, Tokyo, 184-8501, Japan

^r Faculty and Graduate School of Education, Chiba University, 1-33 Yayoi-cho, Inage, Chiba, Chiba, 263-8522, Japan

^s Research Institute of Environmental Geology, Chiba, 3-5-1 Inagekaigan, Mihama, Chiba, 261-0005, Japan

DOI of original article: <https://doi.org/10.1016/j.quascirev.2018.04.022>.

[☆] When this paper was first published, there was an error in the caption for Fig. 5, the correct artwork and legend are printed below.

* Corresponding author. National Institute of Polar Research, 10-3 Midori-cho, Tachikawa, Tokyo, 190-8518, Japan.

E-mail address: suganuma.yusuke@nipr.ac.jp (Y. Suganuma).

<https://doi.org/10.1016/j.quascirev.2018.11.026>

0277-3791/© 2018 The Author(s). Published by Elsevier Ltd. This is an open access article under the CC BY-NC-ND license (<http://creativecommons.org/licenses/by-nc-nd/4.0/>).

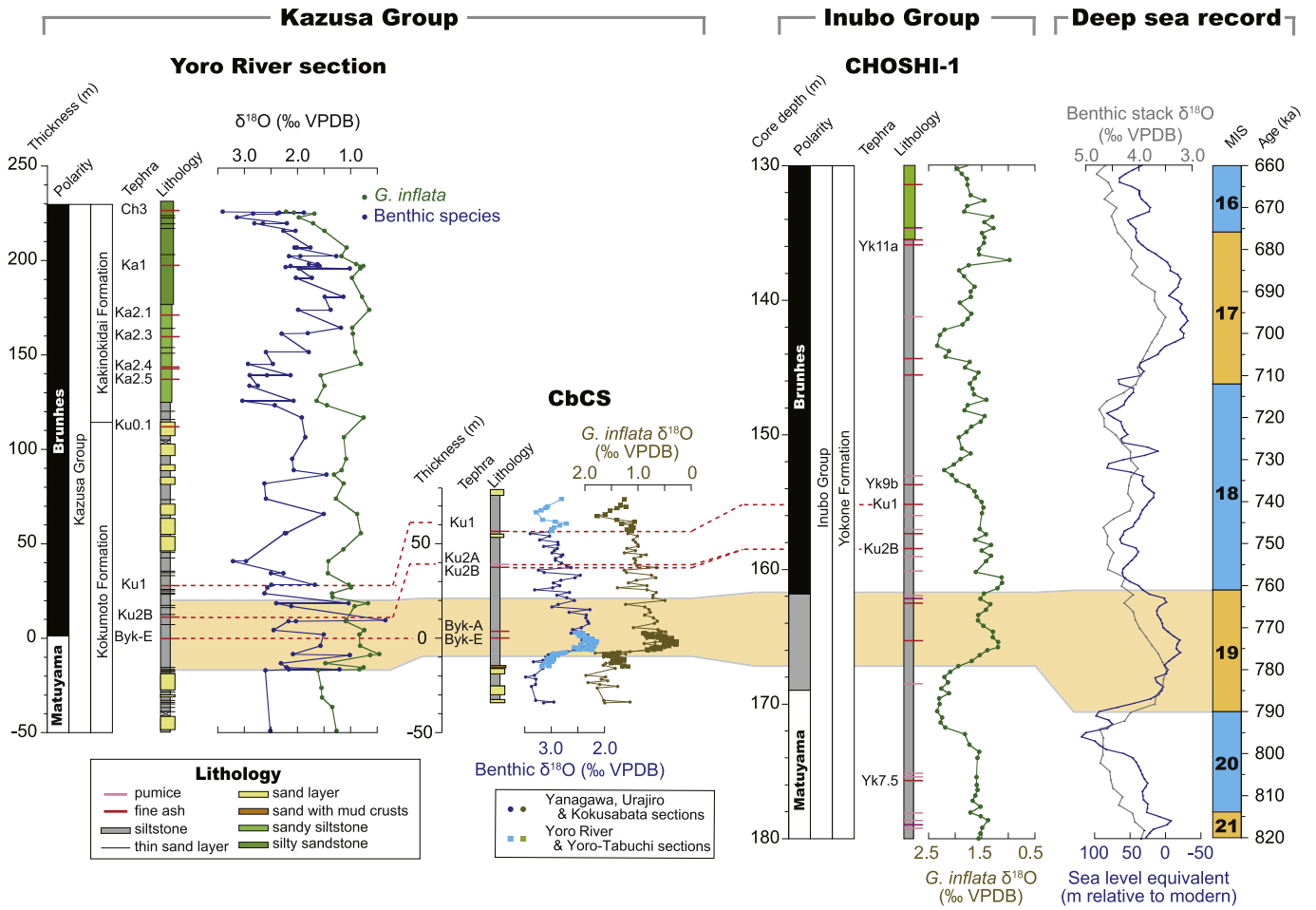


Fig. 5. Chronostratigraphic correlations between the Kazusa Group, including the Chiba composite section (CbCS), and the Inubo Group. The CHOSHI-1 core is thought to recover the homogeneous hemipelagic silt/clay sediments of the Inubo Group (Ozaki, 1958; El-Masry et al., 2002), and the age model is based on visual matching with the sea level proxy of Elderfield et al. (2012). The LR04 benthic stack (Lisiecki and Raymo, 2005) is also shown for comparison. VPDB: Vienna Pee Dee Belemnite, MIS: Marine Isotope Stage. The ages of the MIS boundaries follow Lisiecki and Raymo (2005) and are taken from http://www.lorraine-lisiecki.com/LR04_MISboundaries.txt. To refine marker tephra correlation, we have newly measured major elemental compositions of the volcanic glass shards from these tephra beds (Supplementary Table 1 and Fig. 2). Our data show that the major elemental compositions of Ku1 and Ku2B are similar those of Yk9a and Yk8.5, confirming this correlation. Oxygen isotopes in the CHOSHI-1 core and the Yoro River section are from Kameo et al. (2006) and Pickering et al. (1999), respectively.